HUNGARIAN GEOGRAPHICAL BULLETIN

2012 Volume 61 Number 4

CONTENT

Studies

Literature

Chronicle

Spatio-temporal distribution of dust storms – a global coverage using NASA TOMS aerosol measurements

György VARGA[1]

Abstract

Wind-blown dust and dust storms play important role in several environmental processes of our planet. Geographical distributions and seasonality patterns of major dust source areas were analysed in this paper by using the daily aerosol measurements of NASA's Total Ozone Mapping Spectrometer (TOMS) between 1979 and 2011. Spatial investigations of aerosol maps have confirmed that major source areas can be connected to specific geomorphological environments of distinct arid-semiarid regions with recent pluvial history. Largest dust activity can be observed in the topographical lows of Saharan and Arabian deserts, and in the intermountain, endorheic basins of Central Asia fed by fine-grained material from the adjacent mountain belts. Dust emissions are associated to regional seasonal, meteorological conditions; with typically high dust activity in spring and summer.

Keywords: dust storms, atmospheric dust, satellite measurements, geomorphological environments, meteorology

Introduction

Dust storms and deflated fine-grained aeolian mineral particles (<62.5 μm) are subjects of growing interest due to their multiple influences on climatic and other environmental processes (Harrison, S.P. *et al.* 2001; Kohfeld, K.E. and Tegen, I. 2007; Maher, B.A. *et al.* 2010; Pósfai, M. and Buseck, P.R. 2010; Shao, Y. *et al.* 2011). Wind-blown dust absorbs, scatters and reflects both the incoming shortwave solar and the outgoing longwave radiation, so modifies the energy-balance of our planet. Mineral particles can change the albedo of surface (Arimoto, R. 2001), cloud-formation processes (Rosenfeld, D. *et al.* 2001; Sassen, K. *et al.* 2003), chemical properties of precipitation (Roda, F. *et al.* 1993; Rogora, M. *et al.* 2004) and also have an effect on biogeochemical cycles through Fe fertilization of iron-limited oceanic ecosystems (Ridgewell, A.J. 2002). The far-travelled dust material incorporates

[1] Geographical Institute, Research Centre for Astronomy and Earth Sciences HAS, H-1112 Budapest, Budaörsi út 45. E-mail: varga.gyorgy@csfk.mta.hu

Table 1. Major environmental and climatic factors affecting the formation, size and frequency of dust storms

	Climate and meteorology	Geology and pedology	Geomorphology	Other factors
Formation of dust material	– aridity – temperature (values, distribution and freeze-thaw actions) – precipitation (amount, distribution and intensity) – evapotranspiration	– physical and chemical weathering – grain-size – mineralogical composition – bulk density – soil type – soil moisture content – carbonate content – organic material content	– relief energy – mass movements – aspect – drainage network	– land-use changes – overgrazing – water diversions
Transportation of mineral dust	– air-mass – wind speed – wind direction – convectivity and other vertical movements – precipitation (wet deposition)	– desert and soil crusts	– surface roughness – wind channels – orographic obstacles	– vegetation type and coverage

into the soil-system and increases its clay and fine-silt components even in distant areas. And at last but not least, the increased atmospheric concentration of PM_{10} and $PM_{2.5}$ particles has major effects on human health.

The global annual dust emission of mineral dust deflated from arid-semiarid areas is estimated between 1 and 3 billion of tonnes annually (Tegen, I. *et al.* 1996; Ginoux, P.M. *et al.* 2001; Zender, C.S. *et al.* 2003). Dust loadings of a given area have large annual and interannual variability controlled by several climatic and other environmental changes (*Table 1*).

The monitoring of dust storms and amount of emitted atmospheric dust can be indicative of these changes. In some periods of the Earth's history, the intensity and frequency of dust storms could have increased by several orders of magnitude compared to the present situation (Mahowald, N. *et al.* 1999, 2006; Kohfeld and Harrison, S.P. 2001). Thus, dust records of accumulated aeolian dust deposits (red clay and loess deposits; dust samples of deep-sea sediments; terrestrial material in ice-cores) are of significant importance in reconstructing past climatic and environmental processes, circulation patterns, dust source areas and emissions (Pye, K. 1987, 1995; Pécsi, M. and Schweitzer, F. 1995; Kis, É. and Schweitzer, F. 2010; Kis, É. *et al.* 2011; Újvári, G. *et al.* 2012).

Present paper is aimed at providing information on the geographical distribution and seasonality cycles of dust storms during the investigation period of 1979–2011.

Methods

Nowadays, identification and mapping of major dust source areas can be attained by various satellites, which can provide more appropriate picture on global distribution of dust storms than anecdotal observations of travellers or episodic meteorological observations. Several previous studies have confirmed that daily aerosol index (*AI*) values of NASA TOMS can be used effectively to map spatial and temporal distribution of absorbing aerosols between 70°N and 70°S latitudes (e.g. Prospero, J.M. *et al.* 2002; Washington, R. *et al.* 2003; Engelstaedter, S. *et al.* 2006; Goudie, A.S. and Middleton, N.J. 2006). These sensors (on board of different sun-synchronous NASA satellites) have the longest available global record (since 1978 November) with appropriate spatial (1×1.25 degree) and temporal (daily) resolution (Herman, J.R. *et al.* 1997; Torres, O. *et al.* 1998).

The TOMS aerosol index, as defined by NASA/GSFC Ozone Processing Team, is a measure of how much the wavelength dependence of backscattered UV radiation from an atmosphere containing aerosols (Mie scattering, Rayleigh scattering, and absorption) differs from that of a pure molecular atmosphere (pure Rayleigh scattering). The aerosol index *AI* is defined as

$$AI = 100 \log_{10}\left(\frac{I_{360}^{meas}}{I_{360}^{calc}}\right),$$

where I_{360}^{calc} is the measured 360 nm TOMS radiance, I_{360}^{calc} and is the calculated 360 nm TOMS radiance for a Rayleigh atmosphere (Herman, J.R. *et al.* 1997).

The whole database is actually a huge 3D matrix with latitude–longitude–time dimensions (*Figure 1).* The data-matrix was analysed in MathWorks' Matlab (R2007b) environment by a self-developed algorithm. With the calculations of regional daily means regional time-series were created, which data-series could be analysed by mathematical-statistical methods (identification of annual, interannual and seasonal changes). The global mean maps (e.g. monthly, seasonal and yearly means) were compiled by averaging the whole data-domains; the kriging of maps was processed in Golden Software SURFER 8. The detailed discussion of the source areas was completed with the ETOPO1 1 arc-minute global relief model (Amante, C. and Eakins, B.W. 2009) and with NASA's Blue Marble Next Generation satellite images (Stöckli, R. *et al.* 2005).

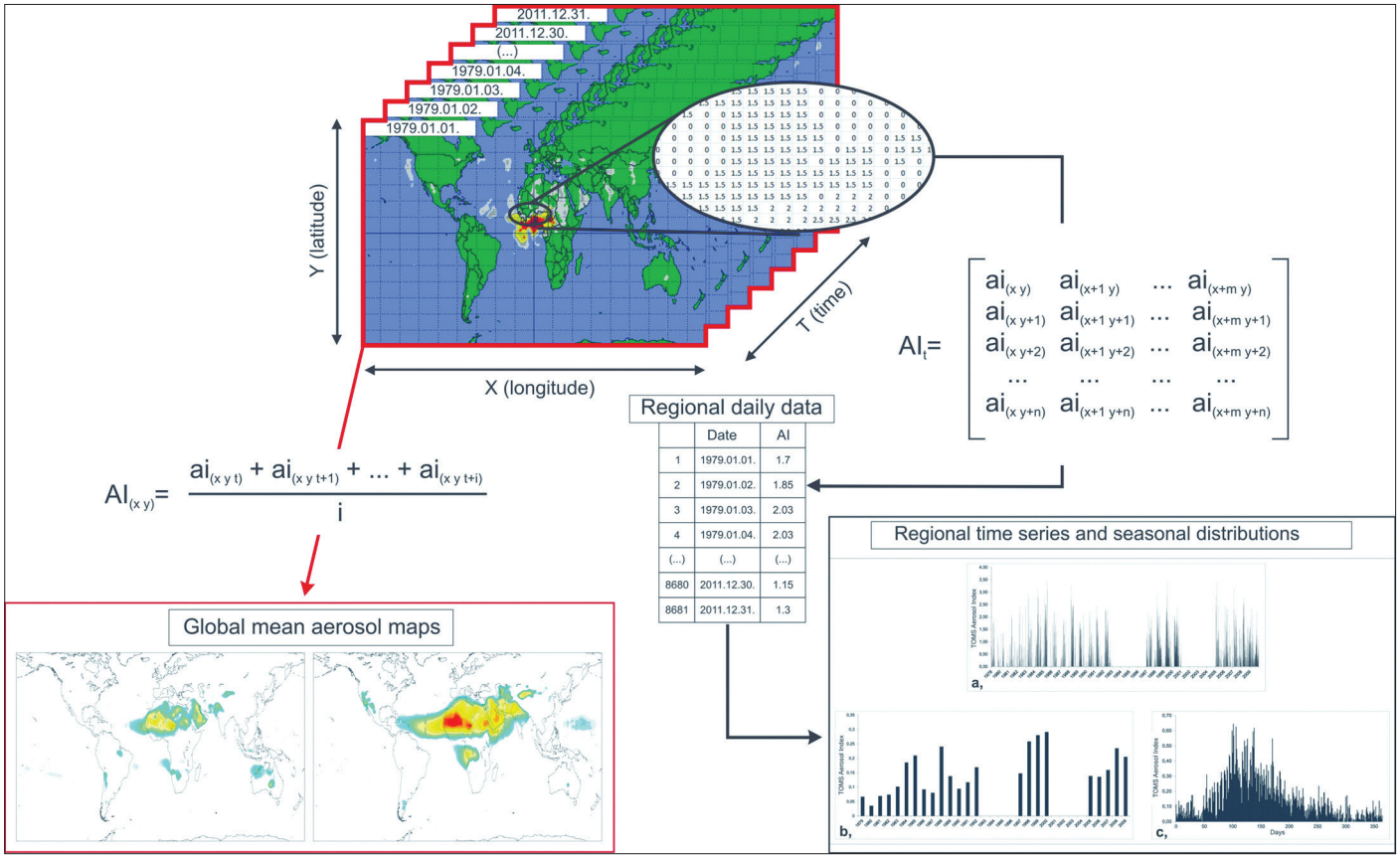

Fig. 1. Schematic illustration of the analyses

Fractional data of 1993 and 1996 (caused by satellite failure), periods with calibration problems of 2001–2004 (Kiss, P. *et al.* 2007) and 2010–2011, and four-yearly leap days (due to the matrix-operations) were excluded from the long-term mean mapping analyses (*Table 2*).

Table 2. The employed periods of TOMS AI data-matrices

Data used	Satellite	Time-series	
01/01/1979–06/05/1993	Nimbus-7	14×365 + 126	5,236 days
06/05/1993–25/07/1996	No data		
25/07/1996–31/12/2000	EarthProbe	4×365 + 160	1,620 days
01/01/2001–31/12/2004	Calibration problems		
01/01/2005–31/12/2009	Aura/OMI	5×365	1,825 days
01/01/2010–31/12/2011	Calibration problems		
01/01/1979–31/12/2011		*23×365 + 286*	*8,681 days*

Global spatial distribution of dust storms

The global mean map of the investigation period (1979–2011) shows the spatial distribution of the most important dust source areas *(Figure 2*). These are situated mainly in the desert, semi-desert regions, where dry, unconsolidated and unprotected fine-grained sediments can be easily lifted by the wind into the atmosphere. Albeit, the mechanisms responsible for silt production under warm-dry conditions have been a matter of scientific debate for many years, triggered by the absence of extent loess regions in the marginal zones of major deserts.

However, recent observations have shown that aeolian and fluvial abrasion, salt and thermal fatigue weathering may also produce large quantity of silt-sized material. Various geomorphological environments (e.g. dry and salt lakes, playas, wadis, ephemeral streams, alluvial fans) are also suitable for substantial dust generation (Assallay, A.M. *et al.* 1998; Wright, J.S. 2001; Smith, B.J. *et al.* 2002). It is important, that water (transportation by ephemeral streams or silt-storage in lacustrine environments) plays substantial role in formation of mineral dust particles, even in arid zones.

Thus, the absence of extensive loess belt around hot desert regions cannot be explained by the insufficient amount of silt-sized material, it is much more likely that loess-formation was prohibited by lack of available vegetation traps for dust. However, long-range transport of small-dust particles (<20μm) with longer atmospheric residence time could have played some role in distant loess-formation processes; e.g. Saharan dust addition to Central and South European loess deposits (Cremaschi, M. 1990; Stuut, J-B. *et al.* 2009).

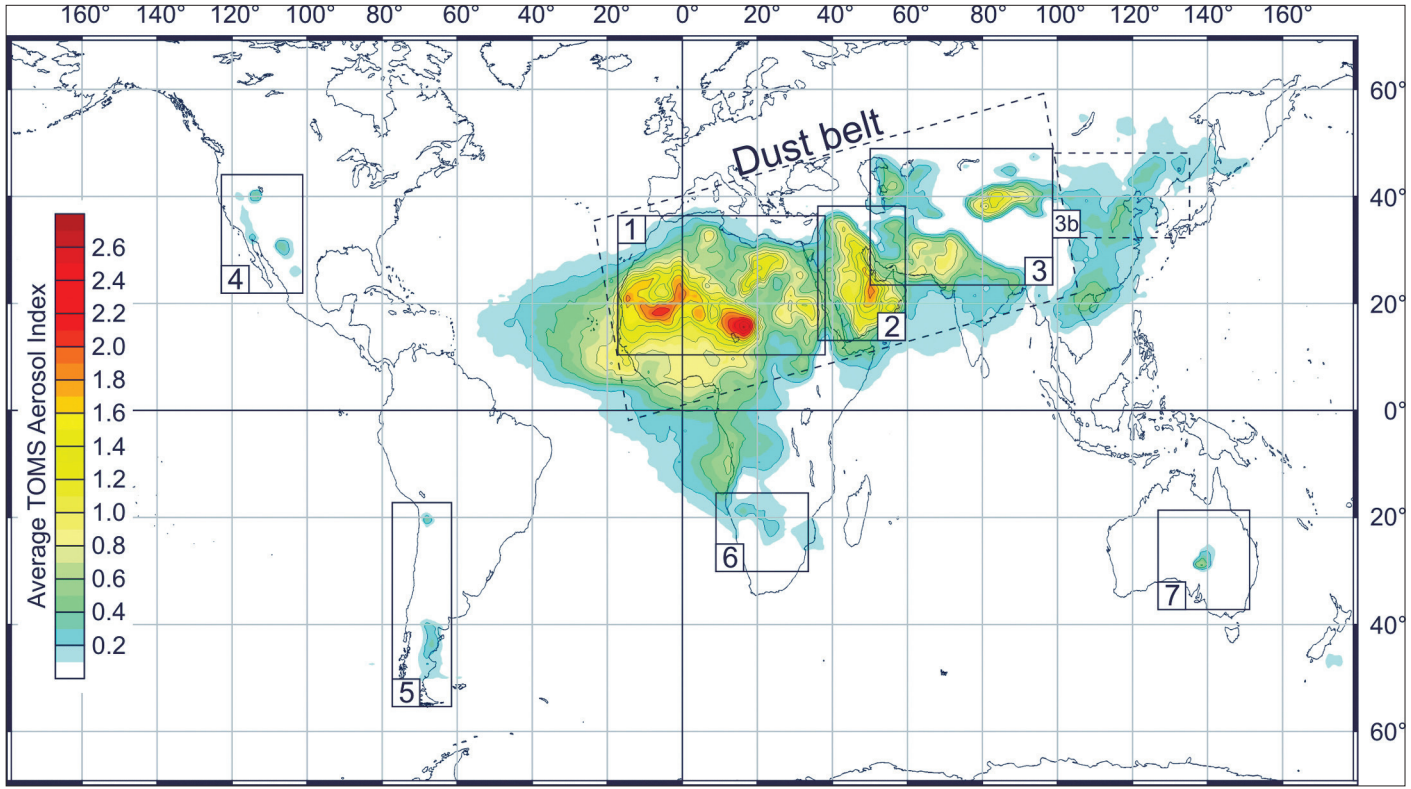

Fig. 2. Global mean map of the measured daily TOMS Aerosol Index values and locations of the discussed major dust source domains. – 1 = Saharan; 2 = Arabian; 3 = Asian; 3b = East Asian; 4 = North American; 5 = South American; 6 = South African; 7 = Australian Domain

As it is indicated by the thick loess blankets, during Pleistocene glacial periods the great ice caps produced huge amount of silty material formed by glacial grinding, but nowadays the low- and mid-latitude arid regions are regarded as the main dust source areas. Due to the spatial availability of the TOMS AI measurements (70°N–70°S), the artic regions with high aerosol emissions are not well represented at the mean maps. The high aerosol values in some equatorial regions and in East Asia are attributable to biomass burning and industrial pollution.

It is clearly visible, that major sources are creating a more or less continuous region from the west coast of North Africa, through the Middle East into the direction of Central Asia. This is the so called "Global Dust Belt" (Prospero, J.M. *et al.* 2002). The average intensity of dust emission and annual frequency of dust storms outside the dust belt are relatively low, concentrated in small distinct areas. The dominance of the source areas located in the dust belt could be noticed much more on the mean TOMS AI distribution diagrams (*Figure 3*).

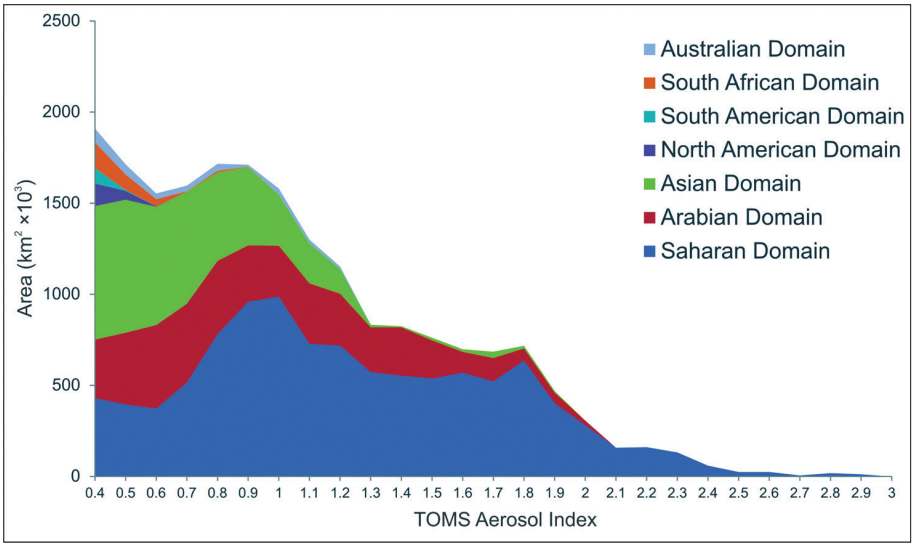

Fig. 3. Areal distribution of different TOMS AI values for the major dust source domains

Temporal distribution of dust storms

The global seasonal cycles of dust storms can be analysed by using the monthly mean aerosol maps (*Figure 4*). The source areas show large temporal variations in their dust emissions, related to various synoptic meteorological and local

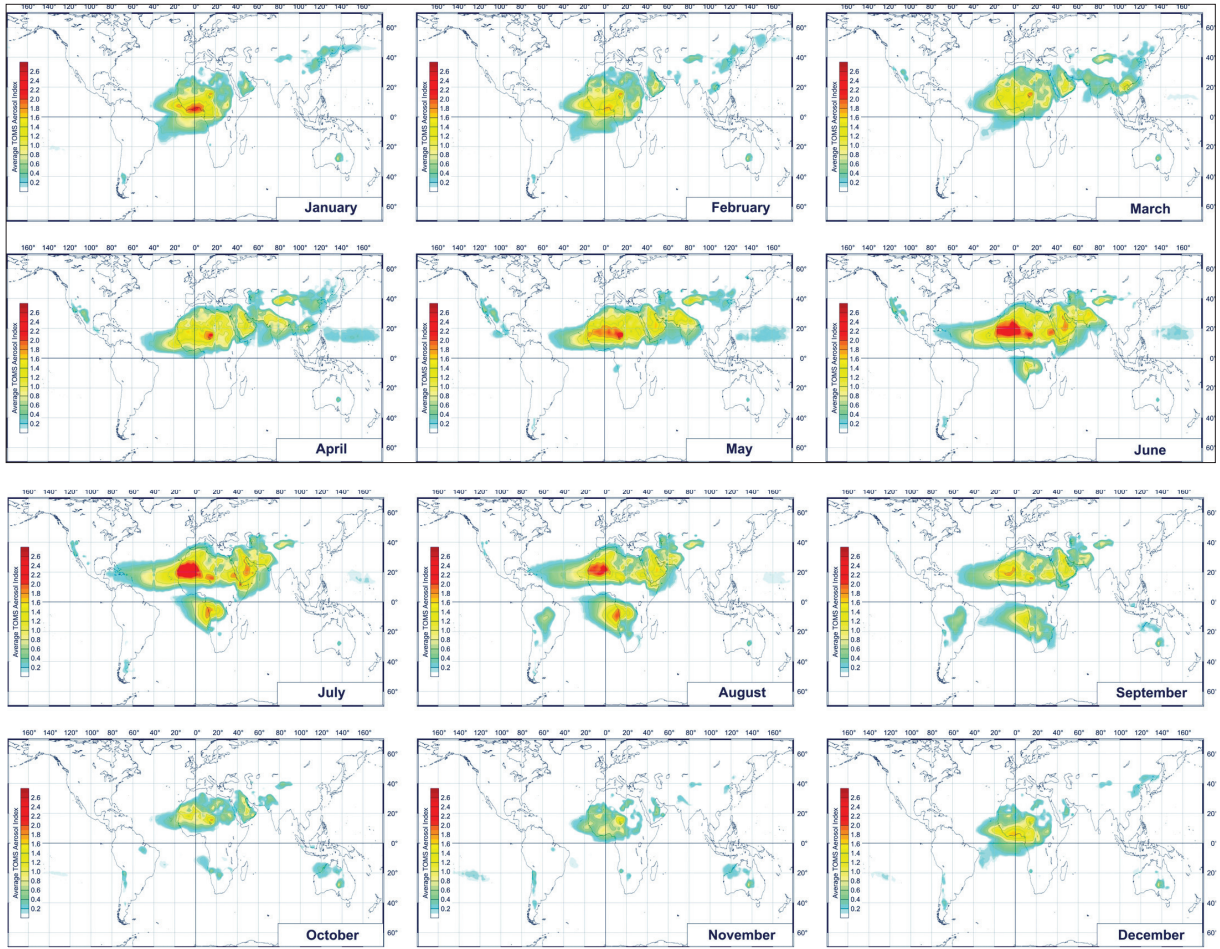

Fig. 4. Monthly mean maps of global TOMS AI values

environmental factors (e.g. distribution of precipitation, thermal convectivity and wind patterns, seasonality of cyclogenesis and other synoptic patterns, vegetation periods etc.).

In generally, it can be stated that in arid areas the seasonal maxima of dust entrainment occur typically during spring and summer, in the periods of highest wind-strengths and thermal convective activity. At some semi-arid and sub-humid, mid-latitude areas the peak of dust activity is at early spring (or late winter) before the vegetation-period, when fields are ploughed and the snow-cover has melted.

Detailed discussion of dust source areas

The appropriate spatial resolution of the satellite measurements allow us to identify distinct source areas on regional scale within the above mentioned major dust source domains and to investigate their common geomorphological and sedimentary environment. The seasonality patterns of all sources were determined by the analysis of regional time-series data. The temporal characteristics of the regions make it possible to assess typical meteorological conditions favourable for dust emission.

Saharan dust source areas

The most intensive and most important dust source areas are situated in the Sahara (and partly in the Sahelian region), responsible for 50–70% of the global mineral dust emission (Ginoux, P.M. *et al.* 2001; Miller, R.L. *et al.* 2004). Dust activity of North African sources shows large temporal variability, except for one region visible all year long, the Bodélé Depression (marked with **1.1** at *Figure 5*).

This area, considered as the largest dust source globally, is located in the large depression northeast from the Lake Chad, once part of the large Lake Mega-Chad (Washington, R. *et al.* 2006). The fine-grained mineral material of the emissions originates from the diatomite deposits of the ancient lakebed, nowadays a series of ephemeral and dry-lakes. The prevailing wind is the northeastern dry trade wind, the Harmattan strengthened by the channelling effect of the Tibesti and Ennedi Mountains.

The dominance of the single general flow direction is clearly demonstrated by the presence of large barchans and barchanoid dunes at the NE parts of the region. The ballistic impact of the saltating sand-sized grains outflowed from dunes plays important role during the entrainment of clay- and silt-sized dust material (Bagnold, R.A. 1941; Pye, K. 1987; Shao, Y. 2008). Though, dust

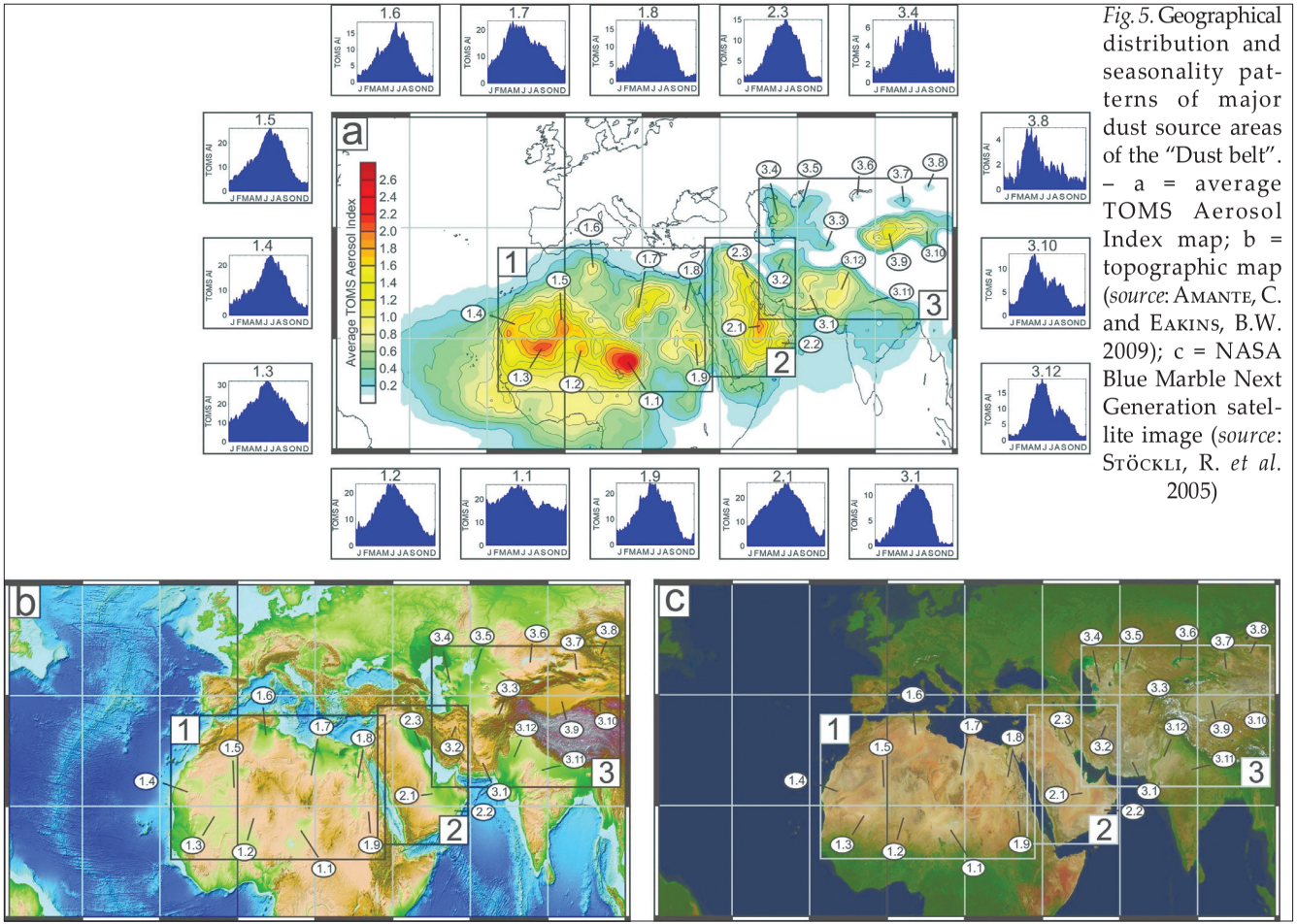

Fig. 5. Geographical distribution and seasonality patterns of major dust source areas of the "Dust belt". – a = average TOMS Aerosol Index map; b = topographic map (*source*: Amante, C. and Eakins, B.W. 2009); c = NASA Blue Marble Next Generation satellite image (*source*: Stöckli, R. *et al.* 2005)

activity persists all year long, the seasonal cycles show some seasonal variability being at the minimum in late summer. Related to the northward migration of the Intertropical Convergence Zone (ITCZ), the wind strength is reduced in July and August, when the convergence of the northerly and southerly winds is situated north from the Bodélé.

An intense isolated spot of high dust activity **(1.2)** can be found in the Azawagh (Azaouak) structural basin framed by the Adrar des Ifoghas, by the Thassili du Hoggar and by the Aïr Mountains. The Azawagh was the catchment area of an ancient northern tributary of Niger River during the Pleistocene pluvial periods (Paris, F. 1995). The dust sources of the region can be associated with alluvial deposits and the system of ephemeral streams originating from the foothills of Ahaggar (Hoggar) and the Aïr.

An extensive dust source is located in the southern part of the Taoudenni Basin NW from the large bend of Niger River and west from the Adrar des Ifoghas **(1.3)**. During the Pleistocene period the area was flooded by Lake Araouane, one of the largest pluvial lakes in Africa (Bridges, E.M. 1990). The salt and diatomite deposits of the enclosed basin can be clearly seen on satellite images. The surface of the ancient lakebed is partly covered by extensive system of barchanoid dunes formed by the prevailing NE trade winds.

The dust emission mechanism of the region is similar to the Bodélé Depression; the intensive deflation of the fine-grained particles of lacustrine deposits is enhanced by the bombardment energy of saltating sand particles. Due to human activities (intensifying irrigation and hydroelectric dam building) the braided distributaries, ephemeral streams and lakes of the Inner Niger Delta could be the next major dust source area of the region (Pearce, F. 2012).

A long narrow band of dust sources is located at the western part of the Sahara **(1.4)**, generally lying at the eastern slopes of gentle hills running parallel to the Atlantic coast. A territory of a series of seasonal streams (with frequent flash floods in the spring) and sebkhas (e.g. Sebkha Ijil) at the pedimented surface of the Adrar Souttouf and Zemmour Massif are acting as the main sources of fine-grained material in this region. Large sand seas (Erg Iguidi and Erg Chech) are situated NE from the area.

Many sources are associated with the large alluvial fans and extensive wadi-system at the W and NW slopes of the Ahaggar **(1.5)**. The Tidikelt Depression at northern part of this region, surrounded by plateaus (the Tanezrouft to the south and Plateau du Tademait to the north), by mountains (Ahaggar and Tassili-n-Ajjer to the east) and by the sand sea of Erg Chech to the west has an extensive ephemeral drainage system including several wadis from elevated regions, seasonal marshes and mud flats (Glaccum, R.A. and Prospero, J.M. 1980).

The dust activity of above discussed four regions shows similar variability throughout the year. The atmospheric dust concentration is at a maxi-

mum in late spring and summer. The dust emission of these sources is primary governed by the migration of the ITCZ and thermal convective activity of the hottest seasons.

An isolated dust hot-spot area can be found in the lowlands south of the Tell Atlas **(1.6)**. The system of salt and dry lakes acts as major source in spring and summer. Dust emission seems to be largest between and to the south of the two largest salt lakes (Chott Melrhir and Chott Jerid) lying north to the Grand Erg Oriental (Prospero, J.M. *et al.* 2002). Dust transportation from the foreland of the Atlas is mostly associated with the formation of Sharav cyclones, generated by the thermal gradient between heated land and cold Mediterranean Sea (Alpert, P. and Ziv, B. 1989; Kalderon-Asael, B. *et al.* 2009). Similar atmospheric circulation patterns are responsible for the dust emission from the dusty area expanding from the northern hillslopes of Tibesti through Cyrenaica to the Qattara Depression **(1.7)**. The main period of dust transportation from the alluvial fans, extensive wadi systems on flanks of topographic highs and ephemeral lakes in the low-lying areas is in spring with a secondary maximum in summer.

Only the low-lying areas next to the north-south trending escarpments along the Nile **(1.8)** and the region of Tokar Delta **(1.9)** can be regarded as important dust sources in the eastern part of Sahara. The alluvial deposits of the silt-laden Baraka River are the parent material of dust storms in the Tokar Delta, where gap winds channelled by the Red Sea Hills transport large quantities of mineral particles into the direction of the Red Sea (Goudie, A.S. and Middleton, N.J. 2006).

Saharan dust is often detectable over the Atlantic Ocean, Mediterranean and Red Sea, and also in the atmosphere of distant areas (*Figure 6*). Typically, four main long-range transportation routes can be distinguished: (1) westward transport of the Saharan Air Layer over the North Atlantic into the direction of North and South America (Prospero, J.M. *et al.* 1970; Swap, R. *et al.* 1992); (2) southward to Gulf of Guinea by the Harmattan (McTainsh, G. and Walker, P.H. 1982); (3) northward to Europe associated to various synoptic meteorological situations (Barkan, J. *et al.* 2005; Engelstaedter, S. *et al.* 2006; Varga, Gy. 2012); and (4) eastward to the Middle East by Sharav cyclones (Alpert, P. and Ziv, B. 1989) or by gap winds at the Tokar Delta (Goudie, A.S. and Middleton, N.J. 2006).

Arabian dust source areas

The second largest dust activity (after the Sahara) can be observed in the Arabian Domain, in the Middle East. Dust plumes cover large areas almost all year long at the Arabian Peninsula and at the Mesopotamian Plain. Three distinct source areas were distinguished in the region. The most prominent dust emission can be detected in the area of salt flats and ephemeral streams at

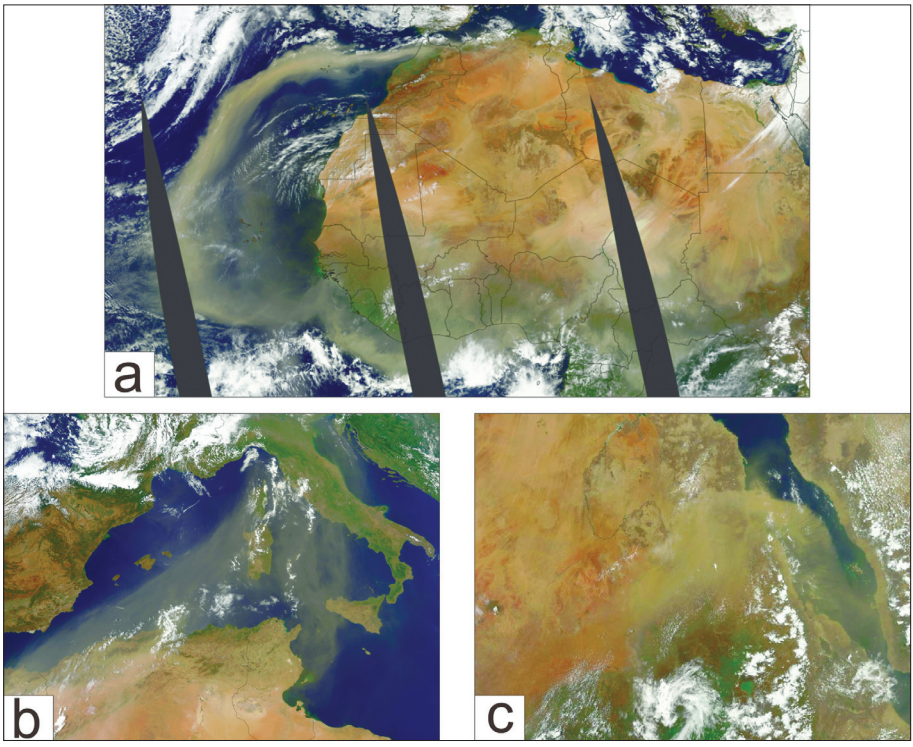

Fig. 6. NASA MODIS satellite images of long-range dust transportation from Saharan source areas. – a = North Atlantic and southward transport (June 6, 2004); b = Saharan dust over the Mediterranean Sea (July 16, 2003); c = North African dust over the Red Sea from the Tokar Delta (June 20, 2012). *Source*: NASA Earth Observatory: http://earthobservatory.nasa.gov/

the eastward facing slopes of Jebel Tuwaiq and over the coastal sabkhas at the low-lying flat terrain running parallel to the Arabian Gulf (**2.1** at *Figure 5*).

The huge sand sea of Rub' al-Khali separates these sources from the dust hot-spot area situated at the SE part of the Arabian Peninsula in Oman **(2.2)**. The isolated circle shaped area with high TOMS AI values is located direct above an inland sabkha system in the low-lying areas fed by wadis from the southern coastal mountainous region of Jebel Dhofar. The dominant dust sources of the Arabian Peninsula are situated in depressions or at the flanks of topographic highs bordered by large sand seas. The main period of dust storms is spring and summer.

Dust activity of the Tigris-Euphrates Basin **(2.3)** can be connected to a different kind of geomorphological environment. At northern territory of the Persian Gulf, floodplain deposits and extensive marshlands of the two large rivers provide the main source of deflated fine-grained mineral material. The seasonal cycle of

dust emission observed by TOMS AI shows same variability; the maximum dust transport occurs in spring and summer and it is at a minimum in winter.

There are several named dust-bearing winds in the Arabian Domain (e.g. belat, simoom, shargi), but the most dusty episodes are caused by the northwesterly shamal winds (Goudie, A.S. and Middleton, N.J. 2006). The high wind-speeds are associated with a steep pressure gradient between the intense summer heat low over Pakistan and Afghanistan and the semi-permanent anticyclonal centre over NW Saudi Arabia (Pye, K. 1987).

Asian dust source areas

Arid-semiarid endorheic basins among high mountain belts, extensive flat terrains, deserts and hyper-continental climate provide suitable conditions for dust emission at several regions of the Asian Domain. Anthropogenic factors also play important role at some places, where the unreasonable constructions of irrigation channels and other agricultural activities have enhanced the dust activity by several orders of magnitude during recent decades.

The most prominent dust sources of SW Asia are associated to shallow saline and dry lakes situated in closed basins, depressions between high mountainous belts and are fed by fine-grained material from these neighbouring elevated regions. According to TOMS AI maps, a cluster of major dust sources are located at the southern flanks of the Makran Coastal Range and in the Sistan (Seistan) Basin (**3.1** at *Figure 5*).

The geomorphological environment of the intermountain basins can be characterized by alluvial fans, wadis, swamps, marshes and a series of shallow lakes, known as hamouns in this region (Middleton, N.J. 1986). The largest ephemeral lakes are Hamoun-e Puzak, Hamoun-e Sabari and Hamoun-e Helmand; these intensive dust sources are the remnants of a once more humid climatic regime at the Hamoun wetlands (Partow, H. ed. 2006). Dust plumes cover large areas also at the NW part of Iranian Plateau, where huge salt flats (kavirs) are covering the wide arid basins of Dasht-e Kavir and Dasth-e Lut deserts **(3.2)**. The small intermountain valley of Fergana **(3.3)** has also a significant dust activity in the region.

Strong katabatic winds funnelled by gaps in the high mountains and thunderstorm downdrafts are causing dust storms especially during the summer months (in July and August), however the dust activity is fairly high from April to October. Dust outbreaks originated from SW Asian sources can often be observed over the Arabian Sea (*Figure 7*).

Several distinct dust sources can be identified at the Turan Plain and at the northern foothills of Central Asian high mountains mostly associated with shallow or dried lakes, ancient lakebeds and alluvial fans (Goudie, A.S. and Wells, G.L. 1995; Prospero, J.M. *et al.* 2002). TOMS AI maps show intensive dust

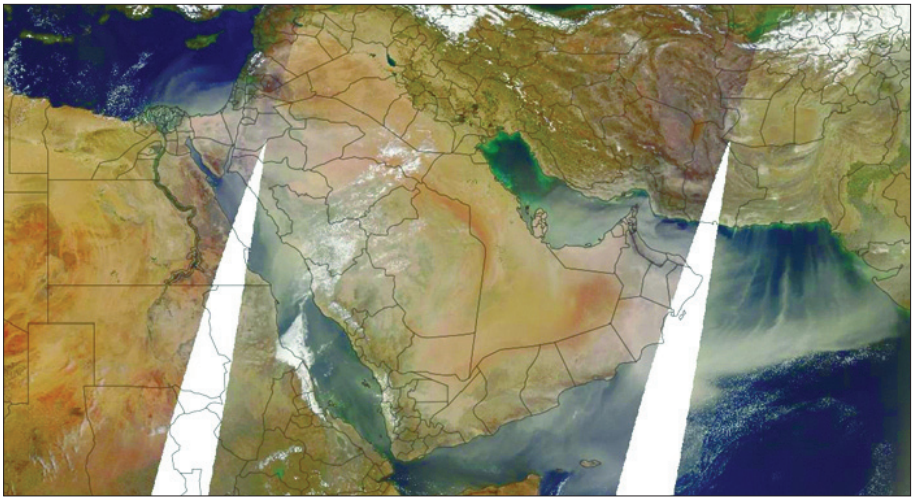

Fig. 7. Massive dust outbreak over the Arabian Sea originated from SW Asian source regions (March 20, 2012). *Source*: NASA LANCE-MODIS Web Mapping Service: http://lance-modis.eosdis.nasa.gov/wms)

emission at the eastern shores of Caspian Sea, direct over the Kara-Bogaz Gol **(3.4)**. The ancient gulf of the lake was dried out as a consequence of construction of an embankment (Gill, T.E. 1996). Another example of anthropogenic environmental disaster areas and another dust hotspot is located in the region, the territory of Aral Sea **(3.5)**. TOMS measurements clearly show that the dried-out deltas of Amu Darya and Syr Darya rivers and the exposed lakebed of shrinking Aral Sea are extensive sources of windblown fine-grained material.

An isolated dust source area is located in the complex drainage basin of Lake Balkhas **(3.6)**. The thick alluvial deposits of the seven feeding rivers and the arid climate of Balkhas-Alakol Basin are providing suitable conditions to effective dust emission. The cold fronts of eastward moving low-pressure atmospheric systems are generating strong winds in the spring, which is the main period of dust activity in the region. Similar synoptic meteorological conditions are responsible for dust storms in the Junggar Basin **(3.7)** and in the Uvs Lake Basin **(3.8)**. These endorheic basins are surrounded by high mountain belts fed by fine-grained material from alluvial fans and ephemeral streams, similarly to other "High Asian" sources.

The largest and most persistent dust source region in Asia is located in the Tarim Basin **(3.9)**. The huge sand sea of Taklimakan desert is bounded by the Himalayan Plateau, Hindu Kush and Tien Shan. At marginal areas of the sandy desert areas extensive ephemeral drainage systems, seasonal lakes and alluvial fans can be identified. The extensive desert area has been a significant

dust source region since the Late Miocene as it is demonstrated by the thick aeolian dust deposits at its flanks and at the Chinese Loess Plateau (Liu, T.S. *et al.* 1985; Zheng, H. *et al.* 2003). TOMS AI measurements show intensive dust emission also at the eastern flanks of the large desert area. These high aerosol values can be connected to the salt flat of Lop Nor and the intermountain Quaidam Basin **(3.10)**.

The dust plumes can be observed all year long over the area, but the highest concentrations of atmospheric dust is most clearly visible on the TOMS AI maps during early spring with a secondary maximum in summer months. Dust material deflated from the Tarim Basin commonly reaches the North Pacific Ocean (Duce, R.A. *et al.* 1980), North America (Jaffe, D.A. *et al.* 1999) or in particular cases, Europe (Grousset, F.E. *et al.* 2003).

Different kinds of dust source areas are lying at the northern part of the Indian Subcontinent. The large alluvial plains of Indus and Ganges **(3.11)** are receiving huge amount of fine-grained material from the bordering Himalayas. The extensive desert area of Thar **(3.12)**, next to the Indus floodplain also serves as a major source area. Dust activity peaks in spring and late summer, with a considerable drop around the arrival of monsoonal rains.

The thickness of Plio-Pleistocene aeolian dust deposits (red clay and loess) exceeds the 300 metres at some places of Chinese Loess Plateau, presenting a once dustier epoch of the region (Liu, T.S. *et al.* 1985).

Nowadays, the area has been regarded also as a territory with high dust loads. However it is difficult to map by TOMS the distribution atmospheric dust and exactly locate the present-day source areas, because of the presence of large amounts of industrial pollutants. According to meteorological data (Middleton, N.J. 1986) and field observations (Derbyshire, E. *et al.* 1998) Gobi, Badain Jaran, Tengger, Ulan Buh deserts and the Hexi corridor are the main sources in Eastern Asia. Due to the intense agricultural activity, the damaged soils of the Loess Plateau are also intense dust sources (Goudie, A.S. and Middleton, N.J. 2006).

North American dust source areas

Dust activity in the region is visible on TOMS aerosol maps from March to August in the SW part of the United States and in northern Mexico (*Figure 8*). Several isolated source regions are situated in the Great Basin bordered by high mountain ranges of Rocky Mountains, Sierra Nevada and Cascades running parallel to the Pacific coast of North America. The internal drainage system of the contiguous intermountain highland basins can be characterized by distinct salt flats, playas, shallow lakes and deep alluvial deposits of fans (Muhs, D.R. in press).

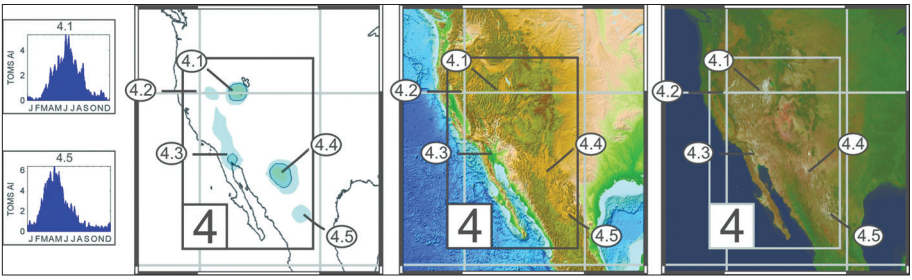

Fig. 8. Geographical distribution and seasonality patterns of major dust source areas in North America

One of the most intense sources is located direct to the SW of Great Salt Lake (**4.1** at *Figure 8*). The lake and the surrounding salt flats of Great Salt Lake Desert, Tule Dry Lake and Sevier Dry Lake are remnant of prehistoric pluvial Lake Bonneville. Similar, but smaller dust source area is located in the Smoke Creek and Black Rock Deserts north to the Pyramid Lake, remnant of Pleistocene pluvial Lake Lahontan **(4.2.)**. Deflation from these ancient, barren lake beds are associated with the passage of strengthening low pressure systems and the related prefrontal winds (Hahnenberg, M. and Nicoll, K. 2012).

Dust emission is also intense from the playa system of Salton Sink in the Coachella and Imperial valleys of southeastern California **(4.3)**. The low-lying pull-apart basin was covered by prehistoric Lake Cahuilla in the Late Pleistocene and Early Holocene (Babcock, E.A. 1974). The steep-pressure gradient between the anticyclonal Pacific High centre and the approaching low-pressure cells creates suitable conditions for dust emission in spring and early summer (Pye, K. 1987).

Two relevant source areas can be observed at the Mexican Altiplano (or Central Mexican Plateau). The plateau area is bounded by the Sierra Madre Occidental and Sierra Madre Oriental; extensive playa systems and alluvial fans are covering its diverse surface. The northern spot of high dust activity is associated with the arid basins and depressions of the Chihuahuan Desert **(4.4)**, while the southern, less active source area is situated in the endorheic basin of Bolsón de Mapimí **(4.5)**. Dust plumes cover large areas in the region during early spring, and as the season progresses dust activity expands to the northwest.

Dust storms at high latitude areas of North America in Alaska (from glacial outwash plains) and in Canadian Prairies, and also at the Great Plains are common; however TOMS measurements cannot represent well these sources, because of aerosol emission is restricted to the lower levels of the troposphere (Herman, J.R. *et al.* 1997).

Three different clusters of dust source areas can be identified by the TOMS AI maps in South America (*Figure 9*). Many isolated sources are associated with the salt flats (salars) located in the internal drainage system of high plateau region of Altiplano flanked by the Oriental and Occidental Cordilleras of the Andes (**5.1** at *Figure 9*). Most remarkable source area is the Salar de Uyuni, the largest salt flat of the Earth. The deep halite deposits of the flats have been accumulated during the Pleistocene pluvials, when large lakes covered the Altiplano's depressions (from north to south: Titicaca, Poópo, Coipasa, and Uyuni) (Placzek, C.J. *et al.* 2011). Nowadays, these ancient lacustrine deposits serve as major source of present-day dust storms in the region, where dusty activity peaks in September–November (Prospero, J.M. *et al.* 2002).

The long narrow band of sources at the eastern slopes of Southern Andes **(5.2)** is active in the second part of the year. Katabatic winds flow out fine-grained particles from alluvial deposits of piedmont area and from extensive series of salt flats, marshes and salinas.

Plio-Pleistocene loess and loess-like deposits cover huge areas in the Patagonia, representing a predominant role of aeolian sedimentation in the region. Recent aerosol maps also show intensive summer and winter dust activity at the Pampas **(5.3)**.

Westerly winds flowing down from the high mountain regions of the Andes transport huge amount of deflated fine-grained particles from glacial,

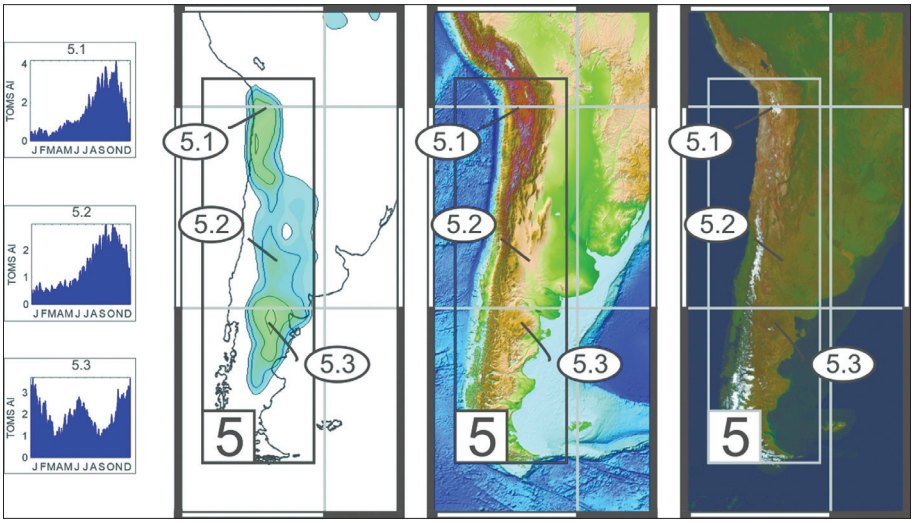

Fig. 9. Geographical distribution and seasonality patterns of major dust source areas in South America

fluvioglacial and volcanic deposits of arid areas lying in rain shadow at easterly slopes of the mountain belt. By its long range transport, Patagonian dust is the main constituent of aeolian deposits trapped in West Antarctic glaciers (Sugden, D.E. *et al.* 2009).

South African dust source areas

Despite to the fact that, there is seasonally huge amount of aerosol particles in South African atmosphere, this is primary related to biomass burnings, and dust emission is restricted to two, relatively small but fairly effective source areas (*Figure 10*). These two dust hot-spots are located over the endorheic basins of Etosha Pan (**6.1** at *Figure 10*) and Makgadikgadi Depression **(6.2)**.

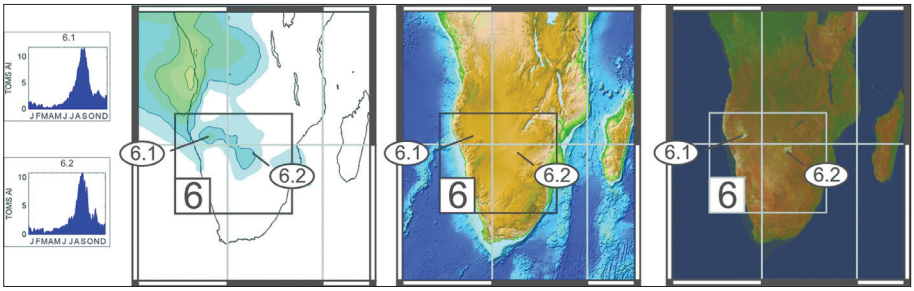

Fig. 10. Geographical distribution and seasonality patterns of major dust source areas in South Africa

Surface of the Etosha Pan is covered by deposits of ephemeral lakes and swamps, and by sediments of former inner delta of Cunene River, which fed the Paleolake Etosha during the pluvial phases of Pleistocene (Goudie, A.S. 1996). Similarly to the other South African source area, Makgadikgadi Depression was also covered by a large pluvial lake in the past. The several salt flats and pans (seasonally flooded by the Boteti River) are the remnants of the Pleistocene Lake Makgadikgadi. Dust activity peaks in August and September, just before the arrival of moister season.

Australian dust source areas

Dust emission of Australia can be connected to one dominant and three weaker source areas (*Figure 11*). Most of atmospheric dust is originated from the mostly dry, large playa system of Lake Eyre basin, a persistent and significant southern hemisphere dust source (**7.1** at *Figure 11*). The fine-grained mineral

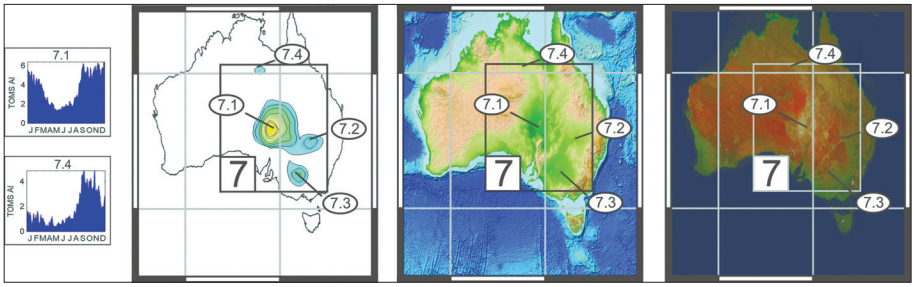

Fig. 11. Geographical distribution and seasonality patterns of major dust source areas in Australia

material of the internal drainage system of playas fed by ephemeral rivers, streams and creeks, floodplain and former aeolian dust deposits are deflated out during austral spring and summer, from September to March.

Other two sources are located in the Murray-Darling Basin. The northern spot of dust activity **(7.2)** can be connected to floodplain deposits of River Darling and its ephemeral tributaries, and to salt swamps (e.g. Caryapundy Swamp). The southern source area is the low-lying region of River Murray **(7.3)**, characterized by floodplain deposits, intermittent salt lakes and swamps. Weak and occasional dust activity can be observed by TOMS over the playas at the SW side of Barkly Tableland **(7.4)**.

Major dust-outbreaks in Australia are related to pre-frontal northerly and postfrontal southerly winds of eastward moving low-pressure systems (Strong, C.L. *et al.* 2011). These two wind-systems determine the offshore dust transportation from Australia into the directions of Southern Pacific and Indian Oceans. The presence of varied aeolian deposits (parna, loess and loess-like deposits, wind-blown sand dunes) shows us, that the region has a long aeolian geomorphological history (Hesse, P.P. and McTainsh, G.H. 2003; Fitzsimmons, K.E. *et al.* 2009).

Summary

Analyses of NASA's TOMS aerosol measurements have demonstrated that the spatial distribution of dust storms are associated to specific geomorphological environments, while emissions show large seasonal variability related to regional meteorological conditions. Areas with high TOMS AI values are lying in arid-semiarid regions, mostly in geomorphological depressions or at flanks of high mountains. The fine-grained dust material of the sources is the product of former fluvial or lacustrine sedimentary environments.

Most of the major sources are situated on remnants of large Pleistocene pluvial lakes, which are nowadays almost totally dried up. The hardened surface of ancient lakebeds can disrupt by bombardment of larger particles, and so the barren deep alluvial deposits are very susceptible to wind erosion. Playas, sabkhas, pans and other ephemeral salt lakes and flats bordered by large sand seas are the largest and most persistent dust source areas of our planet.

REFERENCES

Alpert, P. and Ziv, B. 1989. The Sharav Cyclone: Observations and some theoretical considerations. *Journal of Geophysical Research* 94. 18495–18514.

Amante, C. and Eakins, B.W. 2009. ETOPO1 1 Arc-Minute Global Relief Model: Procedures, Data Sources and Analysis. *NOAA Technical Memorandum NESDIS NGDC* 24. 19 p.

Arimoto, R. 2001. Eolian dust and climate: relationships to sources, tropospheric chemistry, transport and deposition. *Earth-Science Reviews* 54. 29–42.

Assallay, A.M., Rogers, C.D.F., Smalley, I.J. and Jefferson, I.F. 1998. Silt: 2–62 μm, 9–4 Φ. *Earth-Science Reviews* 45. (1–2): 61–88.

Babcock, E.A. 1974. Geology of the northeast margin of the Salton trough, Salton Sea, California. *Geological Society of America Bulletin* 85. 321–322.

Bagnold, R.A. 1941. *The physics of blown sand and desert dunes.* London, Methuen, 265 p.

Barkan, J., Alpert, P., Kutiel, H. and Kishcha, P. 2005. Synoptics of dust transportation days from Africa toward Italy and central Europe. *Journal of Geophysical Research. Atmospheres* 110. D07208. 14 p.

Bridges, E.M. 1990. *World Geomorphology*. Cambridge, Cambridge University Press, 272 p.

Cremaschi, M. 1990. The loess in northern and central Italy; a loess basin between the Alps and the Mediterranean regions. In *The loess in northern and central Italy; a loess basin between the Alps and the Mediterranean region.* Ed. Cremaschi. Milano, Dipartimento de Scienze della Terra dell'Universita degli Studi Milano. Sezione di Geologia e Paleontologia, Nuova Serie 602. 15–19.

Derbyshire, E., Meng, X. and Kemp, R.A. 1998. Provenance, transport, and characteristics of modern aeolian dust in western Gansu Province, China, and interpretation of the Quaternary loess record. *Journal of Arid Environments* 39. (3): 497–516.

Duce, R.A., Unni, C.K., Ray, B.J., Prospero, J.M. and Merrill, J.T. 1980. Long-range atmospheric transport of soil dust from Asia to the tropical North Pacific: temporal variability. *Science* 209. (4464): 1522–1524.

Engelstaedter, S., Tegen, I. and Washington, R. 2006. North African dust emissions and transport. *Earth-Science Reviews* 79. (1–2): 73–100.

Fitzsimmons, K.E., Magee, J.W. and Amos, K.J. 2009. Characterisation of aeolian sediments from the Strzelecki and Tirari Deserts, Australia: Implications for reconstructing palaeoenvironmental conditions. *Sedimentary Geology* 218. (1–4): 61–73.

Gill, T.E. 1996. Eolian sediments generated by anthropogenic disturbance of playas: human impacts on the geomorphic system and geomorphic impacts on the human system. *Geomorphology* 17. (1–3): 207–228.

Ginoux, P.M., Chin, I., Tegen, I., Prospero, J., Holben, M., Dubovik, O. and Lin, S.J. 2001. Global simulation of dust in the troposhere: model description and assessment. *Journal of Geophysical Research* 106. 20255−20273.

Glaccum, R.A. and Prospero, J.M. 1980. Saharan aerosols over the tropical North Atlantic: mineralogy. *Marine Geology* 37: 295–321.
Goudie, A.S. 1996. Climate, past and present. In *The Physical Geography of Africa.* Eds.: Adams, W.M., Goudie, A.S. and Orme, A.R. New York, Oxford University Press, 452 p.
Goudie, A.S. and Middleton, N.J. 2006. *Desert Dust in the Global System*. Springer, 287 p.
Goudie, A.S. and Wells, G.L. 1995. The nature, distribution and formation of pans in arid zones. *Earth-Science Reviews* 38. (1): 1–69.
Grousset, F.E., Ginoux, P., Bory, A. and Biscaye, P.E. 2003. Case study of a Chinese dust plume reaching the French Alps. *Geophysical Research Letters* 30. (6): 1277–1280.
Hahnenberger, M. and Nicoll, K. 2012. Meteorological characteristics of dust storm events in the eastern Great Basin of Utah, U.S.A. *Atmospheric Environment* 60. 601–612.
Harrison, S.P., Kohfeld, K.E., Roelandt, C. and Claquin, T. 2001. The role of dust in climate changes today, at the last glacial maximum and in the future. *Earth-Science Reviews* 54. (1–3): 43–80.
Herman, J.R., Bhartia, P.K., Torres, O., Hsu, C., Seftor, C. and Celarier, E. 1997. Global distribution of UV-absorbing aerosols from Nimbus 7 TOMS data. *Journal of Geophysical Research Atmospheres* 102. (D14): 16911–16922.
Hesse, P.P. and McTainsh, G.H. 2003. Australian dust deposits: modern processes and the Quaternary record. *Quaternary Science Reviews* 22. (18–19): 2007–2035.
Jaffe, D.A., Anderson, T., Covert, D., Kotchenruther, R., Trost, B., Danielson, J., Simpson, W., Berntsen, T., Karlsdottir, S., Blake, D., Harris, J., Carmichael, G. and Itsushi, U. 1999. Transport of Asian air pollution to North America. *Geophysical Research Letters* 26. (6): 711–714.
Kalderon-Asael, B., Erel, Y., Sandler, A. and Dayan, U. 2009. Mineralogical and chemical characterization of suspended atmospheric particles over the east Mediterranean based on synoptic-scale circulation patterns. *Atmospheric Environment* 43. (25): 3963–3970.
Kis, É. and Schweitzer, F. 2010. Dust accumulation and loess formation under the oceanic semiarid climate of Tenerife, Canary Islands. *Hungarian Geographical Bulletin* 59. (2): 207–230.
Kis, É., Schweitzer, F., Futó, I., Vodila, G., Balogh, J. and Di Gléria, M. 2011. Special paleogeographic characteristics and changes in $\delta^{18}O$ values in Upper Pleistocene deposits of the Moravian Plateau. *Hungarian Geographical Bulletin* 60. (3): 247–259.
Kiss, P., Jánosi, I. and Torres, O. 2007. Early calibration problems detected in TOMS Earth-Probe aerosol signal. *Geophysical Research Letters* 34. (7): L07803. 5 p.
Kohfeld, K.E. and Harrison, S.P. 2001. DIRTMAP: the geological record of dust. *Earth-Science Reviews* 54. (1–3): 81–114.
Kohfeld, K.E. and Tegen, I. 2007. Record of Mineral Aerosols and Their Role in the Earth System. *Treatise on Geochemistry* 4. (13): 1–26.
Liu, T.S. *et al.* 1985. *Loess and the Environment*. Beijing, China Ocean Press, 249 p.
Maher, B.A., Prospero, J.M., Mackie, D., Gaiero, D., Hesse, P.P. and Balkanski, Y. 2010. Global connenctions between aeolian dust, climate and ocean biogeochemistry at the present day and at the last glacial maximum. *Earth-Science Reviews* 99. 61–97.
Mahowald, N., Kohfeld, K., Hansson, M., Balkanski, Y., Harrison, S.P., Prentice, I.C., Schulz, M. and Rodhe, H. 1999: Dust sources and deposition during the last glacial maximum and current climate: a comparison of model results with paleodata from ice cores and marine sediments. *Journal of Geophysical Research* 104. 15895–15916.
Mahowald, N.M., Muhs, D.R., Levis, S., Rasch, P.J., Yoshioka, M., Zender, C.S. and Luo, C. 2006. Change in atmospheric mineral aerosols in response to climate: Last gla-

cial period, preindustrial, modern, and doubled carbon dioxide climates. *Journal of Geophysical Research* 111. D10202. 22 p.
McTainsh, G.H. and Walker, P.H. 1982. Nature and distribution of Harmattan dust. *Zeitschrift für Geomorphologie* 26 (4): 417–435.
Middleton, N.J. 1986. *The geography of dust storms*. Oxford, University of Oxford, Doctoral thesis, 591 p.
Miller, R.L., Tegen I. and Perlwitz, J. 2004. Surface radiative forcing by soil dust aerosols and the hydrologic cycle. *Journal of Geophysical Research. Atmospheres* 109. D04203, 24 p.
Muhs, D.R. The geologic records of dust in the Quaternary. *Aeolian Research* (in press)
Paris, F. 1995. Le Bassin de l'Azawagh: pleuplements et civilisations, de néolithique á l'arrivée de l'islam. In *Milieux, sociétés et archéologues.* Ed.: Marliac, A. Karthala, 227–260.
Partow, H. (ed.) 2006. *History of Environmental Change in the Sistan Basin – Based on Satellite Image Analysis: 1979–2005.* Geneva, UNEP Post-Conflict Branch, 60 p.
Pearce, F. 2012. Inner Niger delta set to mimic the Aral Sea disaster. *New Scientist* 213. (2857): 9.
Pécsi, M. and Schweitzer, F. 1995. The lithostratigraphical, chronostratigrphical sequence of Hungarian loess profiles and their geomorphological position. In *Concept of loess, loess-paleosol stratigraphy.* Loess InForm 3. Eds.: Pécsi, M. and Schweitzer, F. Budapest, Geographical Research Institute of HAS, 31–61.
Placzek, C.J., Quade, J. and Patchett, P.J. 2011. Isotopic tracers of paleohydrologic change in large lakes of the Bolivian Altiplano. *Quaternary Research* 75. (1): 231–244.
Pósfai, M. and Buseck, P.R. 2010. Nature and climate effects of individual tropospheric aerosol particles. *Annual Review of Earth and Planetary Sciences* 38. 17–43.
Prospero, J.M., Bonatti, E., Schubert, C. and Carlson, T.B. 1970. Dust in the Caribbean atmosphere traced to an African dust storm. *Earth and Planetary Science Letters* 9. (3): 287–293.
Prospero, J.M., Ginoux, P.M., Torres, O., Nicholson, S.E. and Gill, T.E. 2002. Environmental characterization of global sources of atmospheric soil dust identified with the Nimbus-7 Total Ozone Mapping Spectrometer (TOMS) absorbing aerosol product. *Reviews of Geophysics* 40. 31 p.
Pye, K. 1987. *Aeolian Dust and Dust Deposits.* London, Academic Press, 334 p.
Pye, K. 1995. The nature, origin and accumulation of loess. *Quaternary Science Reviews* 14. (7–8): 653–667.
Ridgwell, A.J. 2002: Dust in the Earth system: the biogeochemical linking of land, air and sea. *Philosophical Transactions of the Royal Society A.* 360. 2905–2924.
Roda, F., Bellot, J., Avila, A., Escarre, A., Pinol, J. and Terradas, J. 1993. Saharan dust and the atmospheric inputs of elements and alkalinity to Mediterranean ecosystems. *Water, Air, and Soil Pollution* 66. 277–288.
Rogora, M., Mosello, R. and Marchetto, A. 2004. Long-term trends in the chemistry of atmospheric deposition in northwestern Italy: the role of increasing Saharan dust deposition. *Tellus B* 56. (5): 426–434.
Rosenfeld, D., Rudich, Y. and Lahav, R. 2001. Desert dust suppressing precipitation: a possible desertification feedback loop. *Proceedings of the National Academy of Sciences USA* 98. 5975–5980.
Sassen, K., DeMott, P.J., Prospero, J.M. and Poellot, M.R. 2003. Saharan dust storms and indirect aerosol effects on clouds: CRYSTALFACE results. *Geophysical Research Letters* 30. (12): 1633, 4 p.

Shao, Y. 2008. *Physics and Modelling of Wind Erosion.* (2nd revised and expanded edition). Springer, 452 p.

Shao, Y., Wyrwoll, K.H., Chappell, A., Huang, J., Lin, Z., McTainsh, G.H., Mikami, M.,Tanaka, T.Y., Wangh, X. and Yoon, S. 2011. Dust cycle: An emerging core theme in Earth system science. *Aeolian Research* 2. 181–204.

Smith, B.J., Wright, J.S. and Whalley, W.B. 2002. Sources of non-glacial, loess-size quartz silt and the origins of „desert loess". *Earth-Science Reviews* 59. (1–4): 1–26.

Stöckli, R., Vermote, E., Saleous, N., Simmon, R. and Herring, D. 2005. *The Blue Marble Next Generation - A true color earth dataset including seasonal dynamics from MODIS*. Published by the NASA Earth Observatory

Strong, C.L., Parsons, K., McTainsh, G.H. and Sheehan, A. 2011. Dust transporting wind systems in the lower Lake Eyre Basin, Australia: A preliminary study. *Aeolian Research* 2. (4): 205–214.

Stuut, J-B.W., Smalley, I. and O'Hara-Dhand, K. 2009. Aeolian dust in Europe: African sources and European deposits. *Quaternary International* 198. (1–2): 234–245.

Sugden, D.E., McCulloch, R.D., Bory, A.J.M. and Hein, A.S. 2009. Influence of Pata-gonian glaciers on Antarctic dust deposition during the last glacial period. *Nature Geoscience* 2. 281–285.

Swap, R., Garstang, M., Greco, S., Talbot, R. and Kallberg, P. 1992. Saharan dust in the Amazon Basin. *Tellus B* 44. (2): 133–149.

Tegen, I., Lacis, A.A. and Fung, I. 1996. The influence of mineral aerosols from disturbed soils on climate forcing. *Nature* 380. 419–422.

Torres, O., Bhartia, P.K., Herman, J.R., Ahmad, Z. and Gleason, J. 1998. Derivation of aerosol properties from a satellite measurements of backscattered ultraviolet radiation: Theoretical basis. *Journal of Geophysical Research Atmospheres* 103. (D14): 17099–17110.

Újvári, G., Varga, A., Ramos, F.C., Kovács, J., Németh, T. and Stevens, T. 2012. Evaluating the use of clay mineralogy, Sr–Nd isotopes and zircon U–Pb ages in tracking dust provenance: An example from loess of the Carpathian Basin. *Chemical Geology* 304–305. 83–96.

Varga, Gy. 2012. Szaharai eredetű por a Kárpát-medence légkörében (Saharan dust in the atmosphere of the Carpathian Basin.) *Földrajzi Közlemények* 136. (2): 106–123.

Washington, R.,Todd, M., Middleton, N.J. and Goudie, A.S. 2003. Dust-storm source areas determined by the Total Ozone Monitoring Spectrometer and surface observations. *Annals of the Association of American Geographers* 93. (2): 297–313.

Wright, J. 2001. „Desert" loess versus „glacial" loess: quartz silt formation, source areas and sediment pathways in the formation of loess deposits. *Geomorphology* 36. (3–4): 231–256.

Zender, C.S., Bian, H.S. and Newman, D. 2003. Mineral Dust Entrainment and Deposition (DEAD) model: Description and 1990s dust climatology. *Journal of Geophysical Research Atmospheres* 108. 4416. 19 p.

Zheng, H., Powell, C.McA., Butcher, K. and Cao, J. 2003. Late Neogene loess deposition in southern Tarim Basin: tectonic and palaeoenvironmental implications. *Tectonophysics* 375. (1–4): 49–59.

The role of slumps in the changing process of soil formation and soil degradation

Csaba FAZAKAS[1]

Abstract

The effects of slumps on soil erosion and soil formation in a Romanian study area, in the Nyárádmagyarós Basin being part of the Nyárádmenti Hills are investigated in this paper. Field and laboratory measurements revealed that slumps particularly intensified linear erosion along the edges of the area of slumps, furthermore, they contributed to the acceleration of erosion in the neighbouring agricultural areas, as well. Slumps contributed to the diversification of the pedological conditions, however, they decreased agricultural usefulness as soils of poor fertility had been formed (stagni-gleyic phaeozems, calcaric regosols). The great ratio of colluvic calcaric regosol proves the erosion of the surrounding areas while two versions of calcaric regosol reflect the locations of different intensity of areal erosion.

Keywords: slump, dissectivity, soil erosion, soil types, Nyárádmenti Hills

Introduction

Slumps are generally studied by geomorphologists, their effects are great on soil formation and degradation therefore pedological investigations are also reasonable in such areas. In this paper the effects of slumps on soil erosion and soil formation are studied in the area of a piedmont basin (Nyárádmagyarós Basin, Romania) *(Figure 1).*

Slumps, special types of mass movements resembling the characteristic forms of the Transylvanian Mezőség are also typical in the Nyárádmagyarós Basin. The clay-marl-sand stratification of the basin and its piedmont basin character help the formation of these landslide types.

Cholnoky, J. (1926) notes that the Transylvanian Mezőség is the "locus classicus" of "slump" formation. He calls the large surface movements on the horizontally stratified slopes of Miocene marly clay slumps. This type of mass

[1] Mures County Office for Pedology and Agrochemistry, Máriaffy Lajos str. 13, Sângeorgiu de Mureş, Romania. E-mail: csfazakas@gmail.com

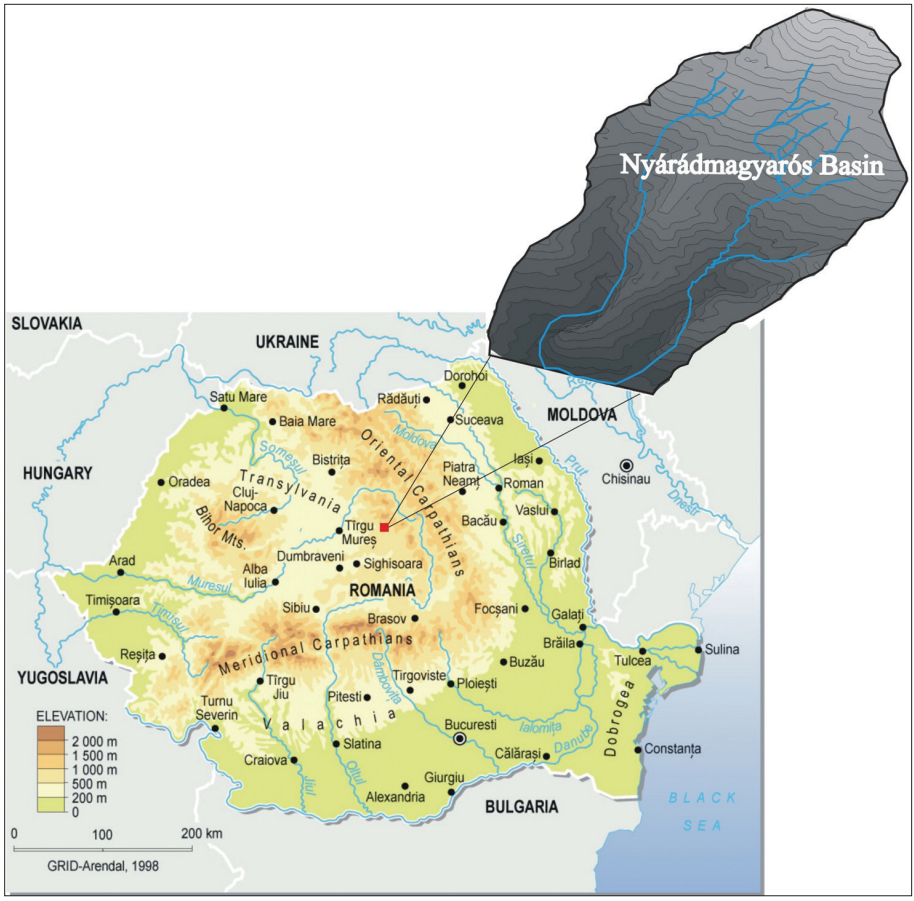

Fig. 1. Location of the Nyárádmagyarós Basin in Romania

movement can be considered as a special form of natural hazard (Szabó, J. et al. 2007). The term slump stands for the deep seated, occasionally rotational surface movements of homogeneous materials (and) with syngenetic slip planes (Sharpe, L.F.S. 1938; Hutchinson, J.N. 1978; Varnes, D.J. 1978; Plummer, Ch.C. and McGeary, D. 1991).

Based on his observations primarily in the Transylvanian Mezőség and on the relevant Romanian literature (e.g. Tövissi, J. 1963; Morariu, T. and Gârbacea, V. 1968), Szabó, J. (1996) thinks that syngenetic slumps "may form not only on slopes of homogeneous material". In his opinion, the landslides formed on the inface slopes which "cross" the anaclinal strata of the asymmetric valleys formed by the non radial dissection (tectonic or erosional) of

the monocline structure developed on the edges of the diapirs in the Mezőség occur on non preformed slip planes although the slope is inhomogeneous. Therefore those obsequent landslides are syngenetic.

This characteristic group of slope mass movements is thoroughly discussed in the Romanian geomorphological literature (Morariu, T. and Gârbacea, V. 1968; Grecu, F. 1985; Jakab, S. 1968; Mac, I. 1997; Surdeanu, V. 1998; Urdea, P. et al. 2008). The publications analyse the initiation conditions and the way of movement of those processes together with their re-occurrence and age. The formation and the erosion of soils are, however, less related to the topic.

The climatic and geomorphological conditions of a region determine the circumstances of slump formation (Lacelle, D., Bjornson, J. and Lauriol, B. 2009). Based on the example given by Burn, C.R. and Friele, P.A. (1988) who besides studying the conditions of slump formation also point to the change of soils on the new surfaces developed as a result of slumps, we try to discover the soil conditions changed as a result of a large slump formed in the area of the Nyárádmagyarós Basin.

Mass movements are not new phenomena in the study area, they were present centuries ago. Most of the hillsides composed of loose clayey and marly sediments in the study area have already experienced slumping or they are currently in movement or exposed to landslides.

Studying slumps in relation to soil erosion was carried out on a relatively large Holocene, already stabilized slump area. The effects of surface dissection due to the formation of the slump, changed slope conditions and soil forming factors are studied in relation to the current condition of the soils of the region.

Field and laboratory analysis of the soils contribute to understanding the influence of changed surface conditions on the formation and deterioration of soils and the extent of the area where slumping affects agricultural land-use.

Material and method

The geomorphological map of the Nyárádmagyarós Basin is based on field survey. The model area studied in details is located in the western part of the map *(Figure 2).*

The grade of dissection was determined by field measurements using a Garmin eTrex Vista GPS and a tape-measure due to the relatively small extent of the study area (126 ha). Data were plotted on a 1:10,000 topographic map with 5 m contour lines applying CorelDraw software. Based on the data and the contour lines, the slope gradient map of the area was constructed, as well.

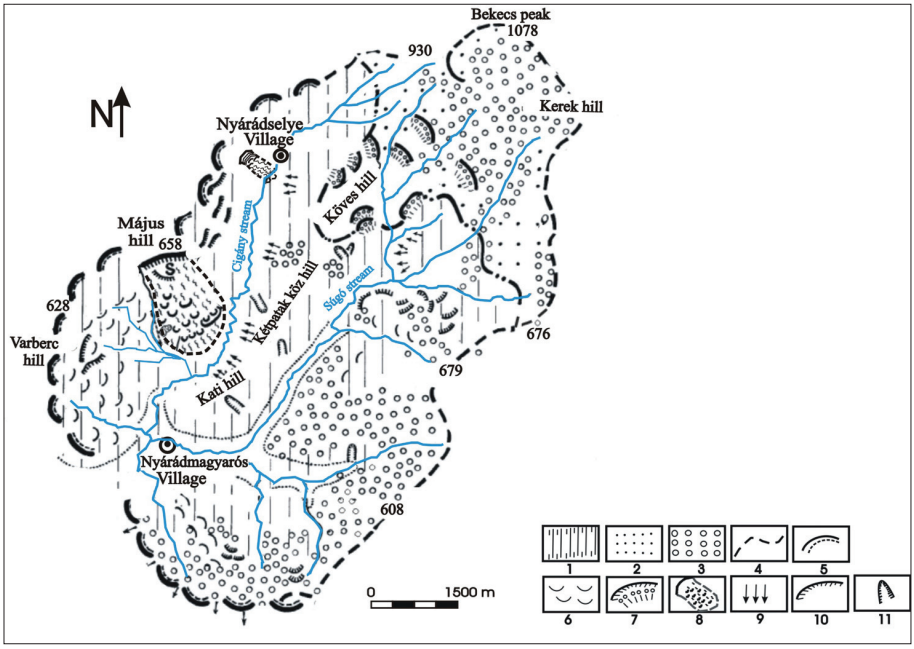

Fig. 2. Geomorphological map of the Nyárádmagyarós Basin. – 1 = Pannonian sediments; 2 = andesite tuffs; 3 = land affected by mass movements; 4 = borderline of the Nyárádmagyarós Basin; 5 = ridges; 6 = translational slides; 7 = step like landslides; 8 = area of the slump at Nyárádmagyarós; 9 = soil flow; 10 = scarps; 11 = erosion trenches

Linear erosional forms on the surface and in the marginal parts of the slump were also measured in order to emphasize the grade of dissection.

Four representative profiles were prepared and described in situ in order to study the soils. Eleven samples were taken from the profiles. Soil type determination was confirmed by drilling at 25 locations using a Prückhauer drilling rod and with the help of 5 control profiles. Soil samples were analysed in the laboratory of the Mures County Office for Pedology and Agrochemistry applying the following methods: pH – potentiometric method; $CaCO_3$ determination – calcimeter with Scheibler's method; humus – Schollenberg's method; nitrogen supply – Kyeldahl's method; phosphorous supply – Egner-Riehm-Domingo method; potassium supply – Egner-Riehm-Domingo method; SB (basoid cation exchange capacity) – Kappen's method; SH (hydrogen ion exchange capacity) – Cernescu's method; grain-size distribution – Kacinski's method. The soil map of the area was constructed based on field and laboratory analyses.

Results

The Nyárádmagyarós Basin is a typical structural basin formed by erosion. The streams running down on the slopes of the Bekecs Hill exposed the monoclinal Pannonian strata in strike orientation forming asymmetric valleys by sliding along the bedding planes.

The Cigány and Súgó streams crossing the basin with NE–SW strike have very variable water levels. Their discharge increases rapidly during spring snowmelt and extended rainfalls and cut into their valley bottoms.

The soil-forming rock in the study area is clay marl which is a clay containing large quantity of carbonic lime. The permeability of this formation is poor as it contains a large amount of swelling smectite type clay minerals which can retain an excessive amount of water. The soil is saturated by water percolating parallel to the surface until late spring. Those characteristics enable the development of such enormous mass movements like the slump at Nyárádmogyorós in certain hydroclimatic conditions.

The Cigány stream was shifted to southeast due to the formation of the slump at Nyárádmagyarós *(Figure 3)* resulting in the occurrence of a steep slope on the left side composed by the slopes of the Köves Hill, the 530 m high Leány Hill extending towards southwest and the 570 m high Kati Hill.

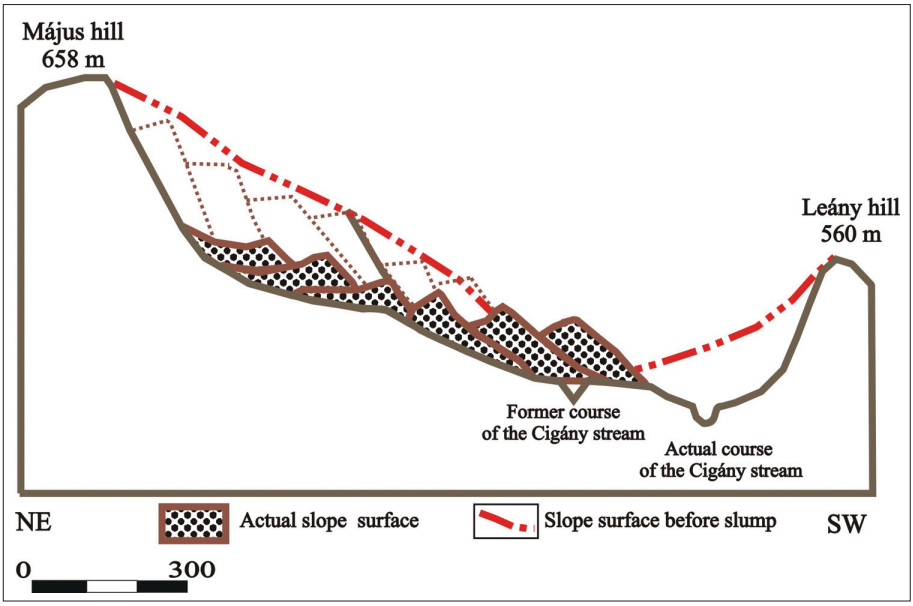

Fig. 3. Sketch of the slope of the Cigány stream prior to the slump

The slope on the right hand side is much gentler, it is the gentle continuation of the cuesta ridge formed along the Várbérc and the Május-tető, sloping towards east, southeast. Its shape is determined by the dip direction of the bedding planes. Its average slope is 10–14° which is roughly the same as the deposition angle of the strata.

On that side the ridge connecting the Május-tető (658 m), Vár-bérc (580 m) and the southern 520 m high points from North to South is a semi-circular form. The area of the slump at Nyárádmagyarós is located in the south-eastern continuation of that semi-circle. The area of slumps at Nyárádmagyarós can be divided into two groups considering the formation and the distribution of slump forms *(Figure 4).*

– the area of the so called twin slumps showing the parallel setting of slump heaps in the three lower belts and

– the upper, younger forms orientated irregularly in the area of the „brother slumps" (Tövissi, J. 1958).

The slump at Nyárádmagyarós is located on the eastern, northeastern limb of the gas dome at Nyárádszereda. Here the average dip of the bedding planes is 9–11° towards the northeast. The infaces are not exposed at the scarp. The scarp is not even located at the infaces. The orientation of the slump is perpendicular to that section of the scarp and has an angle of about 35° with the strike of the strata. Thus the scarp occurred not on the side of the strata but along a line that has an angle of 35° with the dip direction. The slump appeared along a line that has an angle of 35° with the strike of the strata.

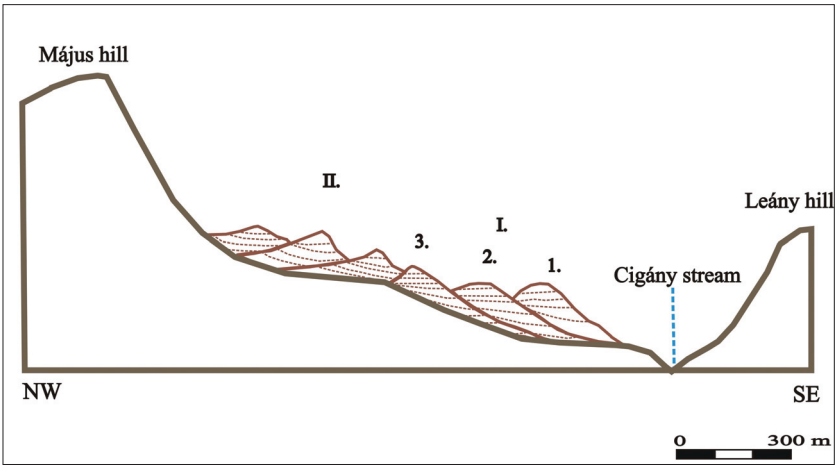

Fig. 4. Distribution of the moved masses on the slope (distorted slope conditions). – I = lower belt: parallel distribution of 1, 2 and 3 slump-head rows ("twin slumps"); II = upper belt: irregular distribution of the slump-blocks ("brother slumps")

No analyses were performed to determine the age of the slump (pollen analysis) in the area, however, the soil conditions and the geomorphological characteristics of the slump suggest a post-glacial (Holocene) age for the formation of the slump.

Simultaneous with the formation of the slump, the slope conditions of the area suffered from a drastic change resulting in a highly increased exposition to new erosion effects (denudation, linear erosion, etc.).

The grade of the dissection is determined by a 40–70 m thick sedimentary rock and soil mixture deposited along a 1,100 m wide scarp. The distance between the youngest scarp and the lowest point of the slump toe is 1,343.8 m. The average slope is 11.3 %. This angle is regarded to be the average slope of the original surface (prior to the formation of the mass movement).The material broke up due to slumping and the newly formed positive and negative forms were further changed by the erosion of external forces.

Currently, the slumped area of 126 ha is characterized by 17 sharp positive forms (hummocks) and the depressions (hollows) between them *(Figure 5).*

The ridges formed as a result of the slump were also disjointed separating into heaps elongated orderly or transversally. Their areas are not large but their effects in deteriorating the agricultural potential of the area are significant. Although the total area of the hummocks is only 11.61 ha, the area which is not good for agricultural activity due to dissection is much larger *(Table 1).*

Table 1. The size of hummocks

Nr.	Area, ha	The relative height of hummocks,* m	Surface of the hummocks,** %
1.	0.09	4.30	0.07
2.	0.14	3.80	0.11
3.	0.18	12.70	0.14
4.	0.28	14.00	0.22
5.	0.34	17.80	0.27
6.	2.09	13.70	1.66
7.	0.26	2.90	0.21
8.	0.28	13.40	0.22
9.	0.57	6.70	0.45
10.	0.51	7.00	0.40
11.	1.53	13.50	1.21
12.	0.27	2.70	0.06
13.	0.10	2.00	0.08
14.	0.56	18.00	0.44
15.	2.32	27.50	1.84
16.	0.67	8.00	0.53
17.	1.52	7.40	1.21
Together	*11.61*	*10.32 (average)*	*9.21*

*According to actual ground. **According to the entire slumped area.

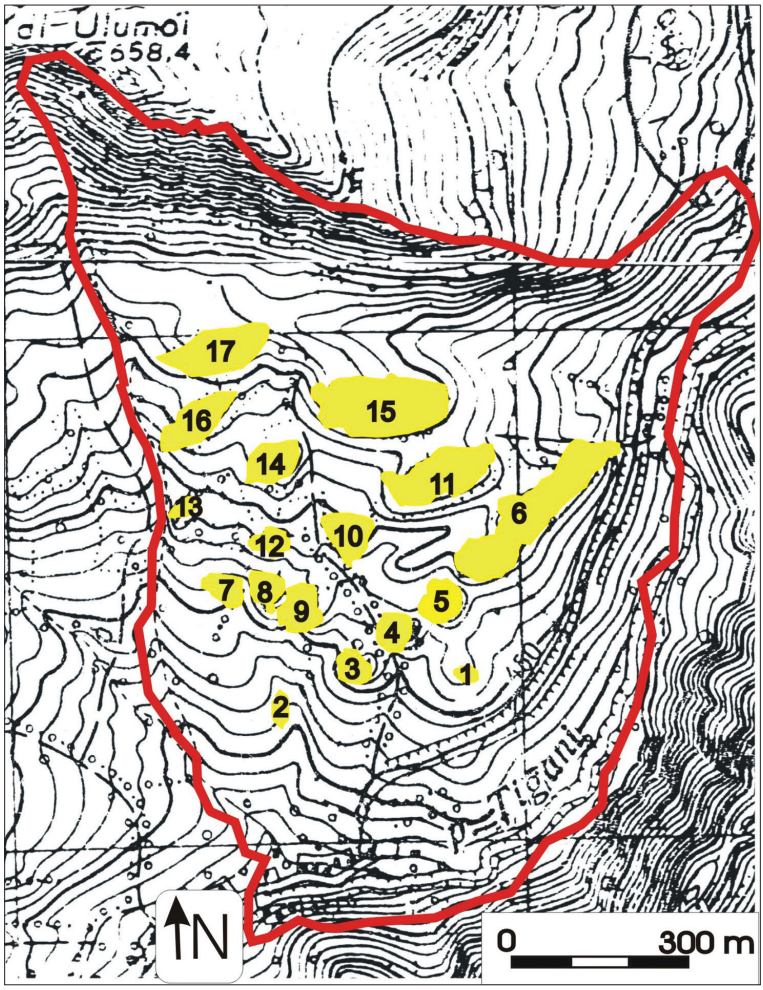

Fig. 5. Dissected and rounded hummocks of the slump surface. (For 1–17 see *Table 1.*)

The figures of *Table 1* show that the sizes of the hummocks vary in a wide range depending on the time of their formations, their locations on the slope and their dissections as a result of their slides. Slumping took place in several phases resulting in one or more slid ridges. This periodicity determined the erosion and the change of the soils and the formation of new soils, as well. Only small patches in the area of the slump have remained to preserve the characteristic soil type of the former surface in an unchanged way/condition.

Considering the occurrence ratio *(Figure 6)* and the spatial distribution *(Figure 7)* of slope gradients, 47% of the area is covered by steep slopes (steeper than 12%) due to dissection. Those steep slopes are considerably exposed to areal erosion.

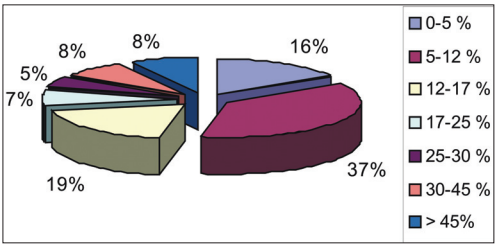

Fig. 6. Percentage of slope gradient categories

Studying the areal soil erosion of the wider environment of the study area, slopes of 8–10% are exposed to areal sheetwash in a smaller extent based on the thickness of the soil horizons. If the effects of weakened soil structure, disrupted vegetation, changed soil moisture conditions and the newly formed linear erosion forms formed as a result of the slumping are considered, it can be stated that the ratio of the area threatened by further erosion effects far exceeds 47%.

Extended steep surfaces were formed on the scarp, in the area of the landslides hummocks, in the foreground of the landslide toe. The originally even, 12–17% steep slope became an area of numerous 65–85% steep hummocks, narrow ridges and dissected talus blocks.

The vegetation cover changed in the slumped area as the ratio of bare surfaces increased and the plant associations changed due to the altered inclination. On the scarp and on the face of the slumped rock and soil blocks, especially on the southern slopes poorly supplied by nutrients, first drought tolerant, thin grassland appeared then bushy vegetation. In the case of the landslide toe, the sliding mass continues its way generally on the gentler foothill. Sliding blocks are piled up into transversal ridges or in different forms of humps. Transversal ruptures run parallel to the ridges.

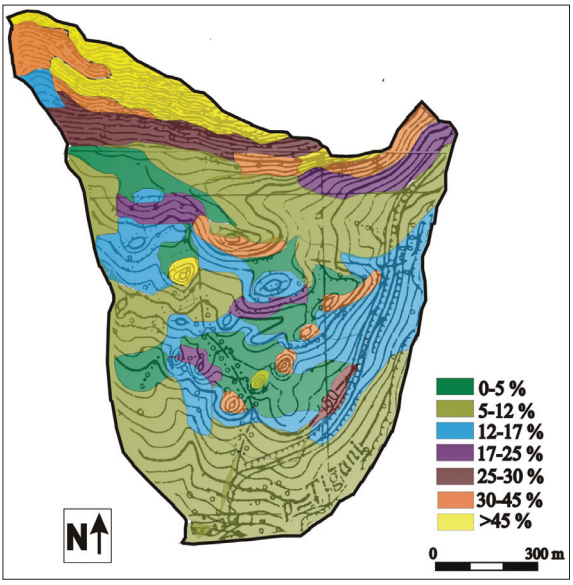

Fig. 7. Slope gradient map of the model area

The internal part of the landslide and the toe even if it is not dissected markedly suffers from sig-

nificant damage in the internal structure, its mass is separated from its surroundings and the effects of linear erosion are intensified, especially in its marginal parts *(Figure 8).*

The total length of the erosion trenches and valleys framing the landslide and discharging the excess water from between the slide humps is 5,077.8 m, their average depth is 2.6 m *(Table 2).*

As erosion valleys incise and the local base level subsides new slope conditions form and new areas become deteriorated experiencing embankment falls and mudslides. The erosion of neighbouring arable lands has been changed by the downcutting of the erosion valley forming the western edge of the slump. A new linear erosion network has developed thus the erosion effect of the slump not only the slumped slope itself but the wider vicinity of the slump, as well.

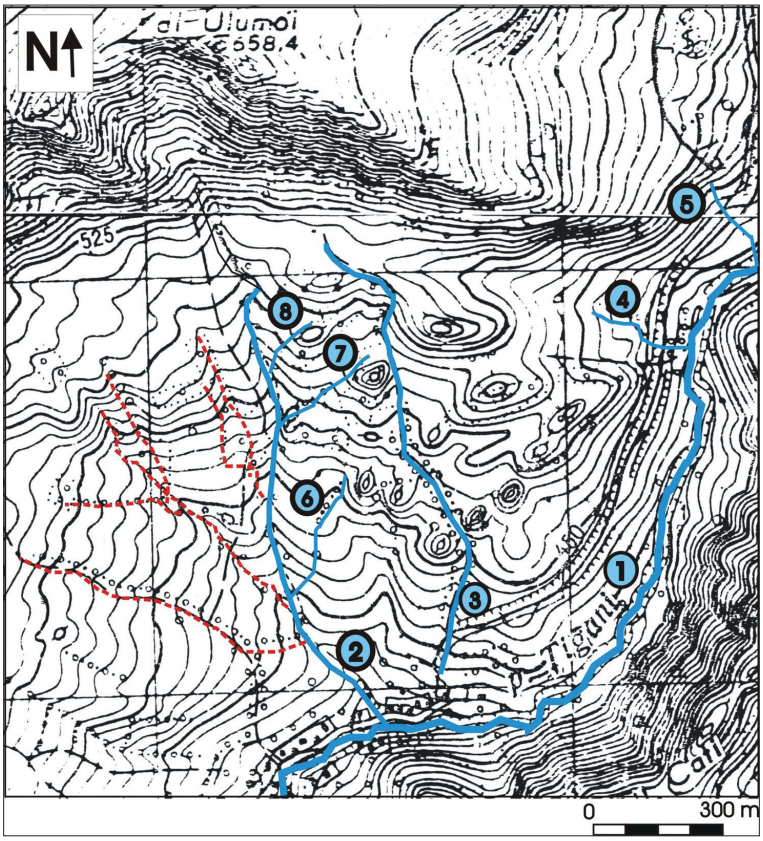

Fig. 8. Linear erosion forms bordering the slump (and developed on it) (see *Table 2*)

Table 2. The size of erosion trenches and valleys

Nr.	Valley classes	Length, m	Average depth m	Maximum depth m	Average steepness %	Maximum steepness %
1.	1	1,611.4	3.7	6.5	11.61	14.60
2.	2	1,402.2	6.4	15.6	9.50	22.50
3.	2	919.8	1.5	2.7	8.90	14.50
4.	2	299.0	1.7	2.2	10.70	17.30
5.	2	228.1	2.1	4.5	14.60	19.40
6.	3	335.9	1.2	1.8	11.40	22.60
7.	3	184.0	2.4	2.9	9.23	10.30
8.	3	97.4	2.0	2.5	13.70	15.80

Studying the soils of the slumped area

Regarding the current stage of soil formation in the study area, we can state that the soils formed in the depressions between the slumped blocks are relatively young, they have no accumulation (B) horizons. In those areas, however, soil formation is significantly influenced by the $CaCO_3$-rich sediment supply arriving continuously from the elevated steep surfaces.

The formation of the slump alters the structure of the removed talus and soil; their horizons are mixed. The altered characteristics of the removed material affect the morphological soil conditions of the soils formed on them together with all characteristics associated with them (water, air and heat budget, organic matter content etc.).

As a result of dissection, the structure of the soil is deteriorated (structure disintegration, the lack of structure), the inner cohesion conditions are changed, soils are mixed, various masses are accumulated or replaced. Mixing of the soil horizons causes changes in the physical-chemical properties of the soils and this way their productivity is also reduced. Based on the field sampling and the laboratory analysis of the samples, 4 soil types have been identified *(Figure 9)* in the area of 126 ha. The high number of soil types in the relatively small area reflects high dissection, i.e. that high grade of dissection was probably the cause of such a variable soil cover.

Considering the ratio of the soil types *(Figure 10),* calcareous colluvic soils with poor humus content and deep humus layer cover most of the surface.

Colluvic calcaric regosol is the characteristic soil type on 48% of the slumped area. This type can be found mainly in the extended depression in the foreground of the main scarp and on the gentle sloping edges of the former slump toe *(Figure 10)*. The great ratio of colluvic calcaric regosol indicates a

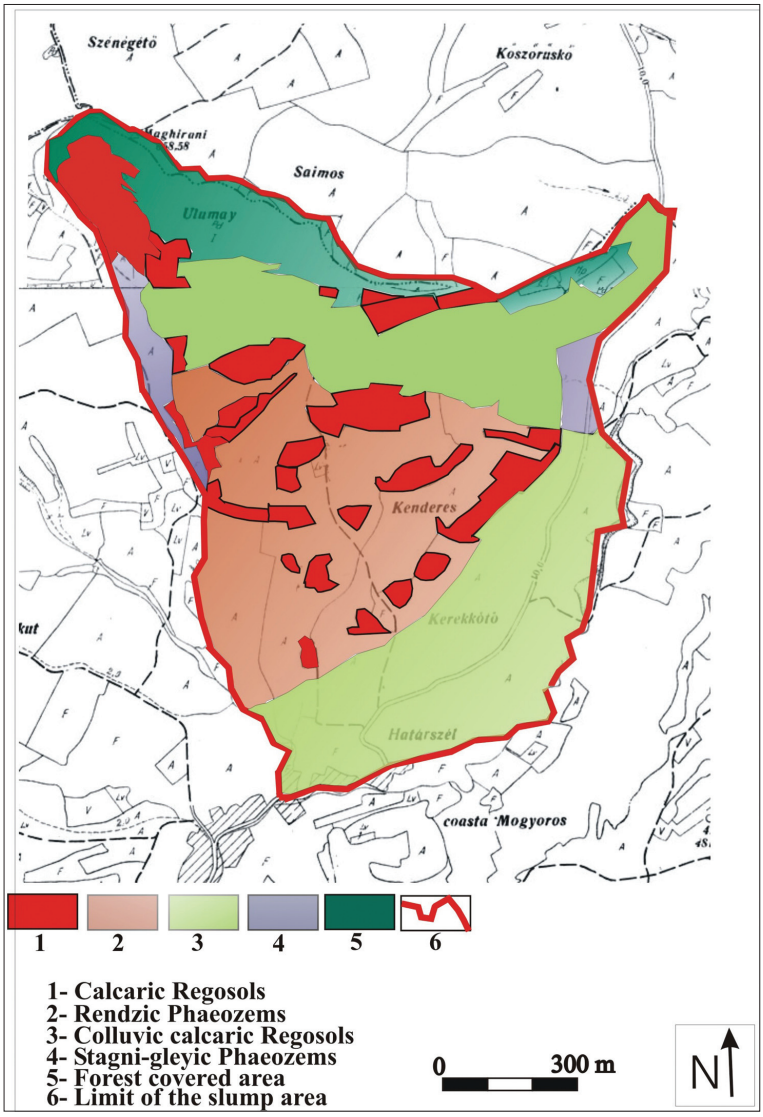

Fig. 9. Soil type map (soils in the areas covered by forest have not been studied)

significant erosion of the neighbouring areas. The material washed from the surrounding highs was accumulated in the lower flat parts or in the depressions of the area and soil formation which started as erosion processes became slower.

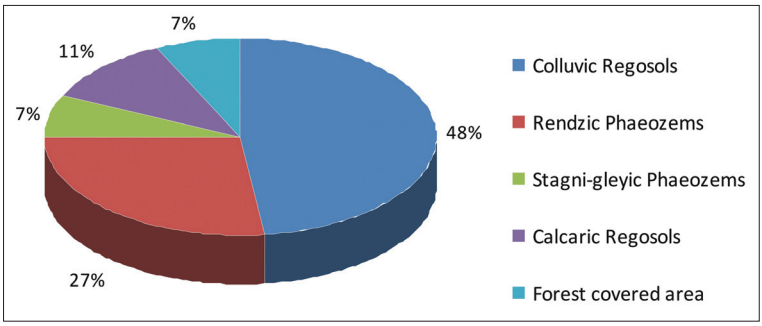

Fig. 10. Soil type ratio of the research area. (Soils in the areas covered by forest have not been studied.)

The horizons of colluvic regosol have no genetic connection as they are not the result of in situ soil formation, they were formed by the accumulation and the mixing of the soil and rock particles washed from the surrounding highs.

The materials of those soil types are originated from the immediate surroundings, their compositions depend on the materials of the soils in the higher areas. In the case of the slumped area at Nyárádmagyarós, the high landforms, the hummocks are greatly eroded in the vicinity of those soils and soil erosion reached the parent rock on the extended surfaces. The materials eroded by water are accumulated in the gentler parts of the slopes and in the valleys in a thickness of 160–200 cm. The thickness of the humus materials can reach 1.2 m, as well.

Their morphological characters are influenced by the rate and the volume of sediment transport and the properties of the transported materials. The structure of the cultivated A horizon is mixed while at greater depths the material is middle-sized and coarse crumbly and blocky. On the structural elements of the Ao_2 horizon, carbonate forms washed in from the upper horizons can be observed. The deteriorated structure and the clayey slope material result in poor water budget.

The nutrient supply of the soil depends on the humus content of the deposited sediments. Since the positive forms eroded significantly have poor nutrient content, the nitrogen supply and the phosphorous supply of the colluvic regosols of the region are also very poor *(Table 3).*

The depressions between the hummocks, the former hollow surfaces are now cultivated by agriculture due to the prolonged erosion of the positive forms. It would be difficult to reconstruct the location of the small drainless lakes (hollow lakes) as they were completely filled, partly as a result of erosion and partly as a consequence of human activity.

Table 3. Laboratory analysis results of colluvic calcaric regosol

Horizon	Depth, cm	pH	$CaCO_3$ %	Humus, %	N %	P_2O_5 Mg/100g	K_2O Mg/100g	Texture			
								sand		Silt	Clay
								Coarse	Fine		
Aa	0–20	7.85	8.0	1.93	0.125	1.4	12.0	4.4	36.5	32.4	26.8
Ao_1	20–37	8.01	9.7	1.02	0.067	0.8	7.5	5.8	36.2	29.5	28.4
Ao_2	37–120	8.04	11.2	0.83	0.057	0.5	7.1	5.0	33.2	27.9	33.7

Table 4. Laboratory analysis results of rendzic phaeozem with medium humus content and moderately deep humus layer

Horizon	Depth, cm	pH	$CaCO_3$ %	Humus, %	N %	P_2O_5 mg/100g	K_2O mg/100g	Texture			
								sand		Silt	Clay
								Coarse	Fine		
Aa	0–26	7.75	0.5	3.20	0.151	1.8	8.6	8.0	26.2	28.1	37.5
A/Cw	26–64	8.03	8.1	1.79	0.080	0.1	8.0	1.2	24.4	36.0	38.5
Cw	64–120	8.11	13.6	–	–	–	–	0.4	20.6	38.4	40.8

The characteristic soils of the former hollow areas are the rendzic phaeozems with medium humus content and moderately deep humus horizons. Their humus content and the thickness of the humus horizons are determined by the original humus content of the depositing sediment. The former presence of the hollow lakes is indicated by traces of gleys in the C horizons of the rendzic phaeozems. Due to the loose, sedimentary soil forming rocks containing carbonic lime, 26 cm deep humus horizon with granular structure was formed containing 3.2 percent organic matter *(Table 4).*

The process of leaching is apparent indicated by the significant decrease of the carbonic lime content of the topsoil compared to that of the soil forming rock. Its humus horizon has a short transition zone towards the soil forming rock.

Since soil denudation erodes the surface continuously and quickly, soil formation appears only in the form of humus formation. Relatively significant vertical extent of the humus layer and the transitional layer suggest decreasing intensity of erosion processes and intensifying humus formation processes. The water supply and the nutrient supply of the covering 27% of the study area are poor and moderate respectively.

The black, leached stagni-gleyic phaeozems (Hanggley-Schwarzboden) covering only a small surface in the study area are regarded to be the most developed soil types which were least affected

Table 5. Laboratory analysis results of the stagni-gleyic phaeozem

Horizon	Depth, cm	pH	pH/KCl	Humus, %	N %	P_2O_5 mg/100g	K_2O mg/100g	V	SH	Texture			
										Coarse sand	Fine sand	Silt	Clay
Aa	0–22	6.4	4.95	2.95	0.157	0.6	13.5	88.2	2.6	4.7	30.1	31.1	34.1
Am	22–54	6.5	5.20	3.02	0.127	0.2	8.0	85.2	3.4	3.3	28.5	31.9	36.2
A/Bw	54–67	–	–	–	–	–	–	–	–	–	–	–	–
Btw	67–180	6.8	5.50	1.57	0.081	0.2	10.0	91.0	2.2	3.0	24.1	29.2	43.7

by the slope debris. It covers 7% of the study area. It is located in the vicinity of the youngest scarp.

Although their formation requires the re-deposition of slope sediments, in our opinion, this re-deposition was areal and took place prior to the slumping based on the thickness of the humus layer. The particles eroded from the surface of the brown forest soils in the more uplifted areas accumulate in the gentler parts and in the negative forms of the slope and significant humus formation takes place in them with the transformation of the remnants of the rich vegetation in the appropriate climatic conditions.

The soil forming rock in the study area is clay marl which is a clay containing large quantity of carbonic lime. The permeability of that formation is poor containing large amount of swelling smectite type clay minerals which can retain excessive amount of water.

Its profile is very deep, horizon C appears generally at around 2 metres. Its humus layer is situated way below horizon A. Its Am horizon containing uniformly high ratio of humus can be divided into two parts *(Table 5).*

The traces of water effect cannot be observed or only in insignificant scale in the upper 0–54 cm. The frequent and tiny iron peas in the lower part indicate marked occurrence of meadow processes. The texture of the stagni-gleyic phaeozem is adobe or clayey adobe. Its upper layer is small or medium grained while its accumulation level is coarse polyhedral. The accumulation layer can be divided into two parts. The upper part is darker, saturated by humus with many iron freckles and iron peas, the lower one is free of the traces of water effect.

Its water budget has disadvantageous and preferable properties, as well. It has low permeability, its dead-water content is high and its water retaining capacity is very good which can be very useful in years of drought. Its characteristic property is saturation with water running within the soil parallel to the surface until late spring. Snowmelt following the cold season characterised by precipitation surplus and abundant rains in spring all intensify the slump triggering property of the stagni-gleyic phaeozem.

Table. 6. Laboratory analysis results of the calcaric regosol

Horizon	Depth, cm	pH	$CaCO_3$ %	Humus, %	N %	P_2O_5 mg/100g	K_2O mg/100g	Texture			
								Coarse sand	Fine sand	Silt	Clay
Ba	0–18	7.51	15.5	1.75	0.122	2.2	11.5	13.1	52.2	14.3	20.4
B	18–40	7.90	16.0	0.77	0.055	1.1	9.4	6.9	40.5	21.6	31.0

Its humus content in the upper layers is almost 3% *(Table 5)*. It is well supplied by nutrients but those are released more difficultly in wetter than normal years. Its base saturation is over 80 % while its pH value is over 6. The soil is very sensitive to the cultivation period as the optimal cultivation period is very short when cultivation is possible in reasonable quality. The preferable productivity of the soil is striking in dry years following a dry autumn. This soil type resists long summer drought the most.

One of the most important soil types of the study area is calcaric regosol despite its small spatial ratio as its presence reflects the locations of areal erosion well. That soil type develops on the steep slopes of the hummocks and the scarp.

Since the soil forms on the exposed loose sedimentary rocks, the process of soil formation is impeded by neither the lack of weatherable material nor the transportation of the little weathered material away, but the rapid and constant denudation of the surface. The continuous effects of soil formation and biological processes for a longer term are blocked by erosion processes. Humus development is present only at a shallow depth in the soil profile.

The transformation of the soil forming rock at greater depth is not possible, because soil denudation carries away the already transformed material and new material is continuously supplied for the soil forming processes. The soil layer, i.e. the humus layer does not exceed the thickness of the cultivated layer in actively cultivated areas *(Table 6)*.

At places the soil forming rock is exposed from under the completely denuded soil, however, the development of the bare rock into new soil is impeded by continuous erosion. That soil is denuded in such extent by erosion or deteriorated so much due to human activities that the characteristics and the diagnostic signs of the original soil cannot be identified.

Its humus layer does not reach a thickness more than 20 cm at places, its organic matter supply is ensured by the poor herbaceous, bushy and occasionally – in the area of the scarp – arborescent vegetation, however, it never accumulates as it is continuously washed away due to the steep slopes. There are spatial differences in (case of) that soil type caused by the different intensity of erosion, as well. Along

the main scarp and on the slope-ward side of the hummocks where the angle of slopes exceed 25% the complete denudation of the soil can frequently be detected resulting in bare lands (completely denuded soils) which cannot be utilized in any way. Those lands make up 6% of the total area. Most of those lands cannot be utilized not even as hayfields, nor as grazing lands. Further degradation of their surface could be reduced by planting arborescent vegetation.

On the gentler slopes of the hummocks degradation is of smaller grade. In those areas earthy, bare soils are formed as well, however, thin humus layers of 15–25 cm thickness can be observed. The rock near the surface is soft, covered by the network of plant roots therefore reasonable quantity of crop of soil protecting plants can frequently be harvested from them applying nutrient supply of appropriate quantity and quality. Such lands are often drawn into agricultural cultivation. It is recommended, however, to grow perennial vegetation which improves the soil, i.e. mainly forage plants or to utilize such areas for grazing.

Conclusions

Based on the investigation of the morphology of the slumped area, it can be stated that variable relief conditions were produced by the mass movement(s) with steep slopes which increased potentially the risk of both linear and areal erosions. The fact that linear erosion was intensified at the edges of the slumped area extending over the agricultural areas beside the slumped area was proved based on maps and analyses, as well. Based on the quality of the soils of the study area, it can be stated that although high ratio of the area is characterised by the accumulation of material washed from the positive landforms of the area, soils with thin humus layers, small humus content and poor nutrient supply can be found on those lands due to the quantity and continuity of erosion together with the quality of the washed material. Although the productivity of those soils could be improved by nutrient supply reduction. The halting of further erosional effects is a long-term and expensive task.

The dissected area together with the depressions between the hummocks and the former hollow surfaces are unsuitable for mechanized cultivation. The economic justification of their cultivation is weak.

Blocking the advancement of linear erosion forms could be achieved by breaking their longitudinal profile by cross barriers impeding in this way the further incision of the erosion trenches and the development of new trenches and valleys.

Acknowledgement. The research was carried out with the support of TÁMOP-4.2.2.B-10/1 project.

REFERENCES

Burn, C.R. and Friele, P.A. 1989. Geomorphology, Vegetation Succession, Soil Characteristics and Permafrost in Retrogressive Thaw Slumps near Mayo, Yukon Territory. *Arctic* 42. (1): 31–40.

Cholnoky, J. 1926. *A földfelszín formáinak ismerete (Morfológia)* (The knowledge of the forms of the Earth's surface (Morphology). Budapest, 295 p.

Grecu, F. 1985. Clasificări şi tipuri de alunecări de teren din Depresiunea Transilvaniei. (Classification of landslide types in the Transylvanian Basin) *Revista Terra* 3. 15–17.

Hutchinson, J.N. 1988. *General report: Morphological and geotechnical parameters of landslides in relation to geology and hydrogeology*. Proceedings of the fifth international symposium on landslides, Rotterdam, Balkema, 3–35.

Jakab, S. 1983. Factori favorizanţi ai alunecărilor de teren din Dealurile Târnavelor (Susceptibility factors of landslide formation in the Tarnave Hills region). *Studia Scientarium Naturae* 11–12. (1): 18–26.

Lacelle, D., Bjornson, J. and Lauriol, B. 2009. *Climatic and Geomorphic Factors Affecting Contemporary (1950–2004) Activity of Retrogressive Thaw Slumps on the Aklavik*

Mac, I. 1997. Type of Landslides from the Transylvanian Depression with Differetiated Effects on the Morphology of the Slopes. *Studia Univ. Babeş-Bolyai Seria Geographia* 42. (1–2): 5–7.

Morariu, T. and Gârbacea, V. 1968. Deplacements massifs de terrain de type glimee en Roumanie. *Revue Roumaine de Geologie, Geographie, Geophisique, Serie de Geographie* 12. (1–2): 13–18.

Plateau, Richardson Mountains, NWT, Canada. Wiley InterScience (www.interscience.wiley.com) DOI: 10.1002/666 p.

Plummer, Ch.C. and McGeary, D. 1991. *Physical Geology.* Fifth edition. Wm. C. Brown Publishers, 197 p.

Sharpe, C.F.S. 1938. *Landslides and related phenomena*. New York, Columbia University Press, 136 p.

Surdeanu, V. 1998. *Geografia terenurilor degradate. I. Alunecări de teren* (The Geography of degraded lands. I. Landslides). Cluj-Napoca, Editura Presa Universitară Clujeană, 274. p.

Szabó, J. 1996. *Csuszamlásos folyamatok szerepe a magyarországi tájak geomorfológiai fejlődésében.* (Landslides in the geomorphic evolution of landscapes of Hungary). Debrecen, Debreceni Egyetem, 221 p.

Szabó, J., Lóki, J., Tóth, Cs. and Szabó G. 2007. Természeti veszélyek Magyarországon (Natural hazards in Hungary). *Földrajzi Értesítő / Hungarian Geographical Bulletin* 56. (1–2): 15–32.

Tövissi, J. 1963. Alunecări de teren în regiunea comunei Măgherani (Landslides of the Măgherani region). *Studia Universitatis Babeş-Bolyai, Series 1.* 1–8.

Urdea, P., Ardelean, F., Onaca, Al. and Ardelean, M. 2008. *Deep-seated landslides (glimee) in the Saschiz and Şoard-Secuieni area. Geophysical investigations.* Braşov, IAG Regional Conference on Geomorphology, 15–26 Sept. 2008. 32–33.

Varnes, D.J. 1978. Slope movement types and processes: In *Landslides: analysis and control*. Eds. Schuster, R.L. and Krizek, R.J. Washington DC, Transportation Research Board Special Report 176. National Academy of Sciences, 11–33.

Water temperatures of the Danube and Tisza Rivers in Hungary

György LOVÁSZ[1]

Abstract

Based on a 60-year long hydrological observation series from the Hungarian Hydrological Service (between 1951 and 2010), the monthly mean water temperatures of both largest rivers in the Carpathian Basin, the Danube and the Tisza, important for a range of practical considerations, are studied. The monthly extremes in water temperatures are explained by the different climatic conditions in the drainage basins of the rivers: the Danube basin upstream its entrance to Hungarian territory with a marked Atlantic and the Tisza basin with a strong continental character. Changes are followed along the Hungarian stream sections. Trends in water temperature change are established and interpretations are sought with consideration to the climate change trends predicted by climatologists for Hungary. The trends are more clearly manifested for the Danube catchment than for the Tisza catchment. Within the outlined overall trends, positive and negative singularities are also identified for the coldest and hottest months and their occurrence is also analysed in regional contrast.

Keywords: water temperature, air masses, climate change, singularities

Introduction

In the Hungarian literature analyses of river water temperatures first appeared in the second half of the 19th century and included data from the observations on the Danube (Greguss, Gy. 1866). In the early 20th century observations on the water temperature of the Tisza River were also published (Pasteiner, D. 1905). In the mid-20th century a synthesis based on a 5-year time series of observations on the temperature conditions of standing waters and streams in Hungary (Lászlóffy, W. 1956).The observation network has significantly expanded since 1950: it has become ever denser and, in addition to major rivers, measures began on smaller watercourses too. 60-year series are available and allow analyses of broader thematics.

[1] Professor emeritus, Institute of Geography, University of Pécs, H-7624 Pécs, Ifjúság útja 6. E-mail: gyuresz@gamma.ttk.pte.hu

The present study is based on data from the observations of the Hungarian Hydrological Service for two stations on the two largest rivers: one at entering and another at leaving Hungarian territory. The Danube enters Hungary at Dunaremete and the Tisza near Tiszabecs, while the Danube leaves Hungary downstream of Mohács and the Tisza downstream of Szeged *(Figure 1).*

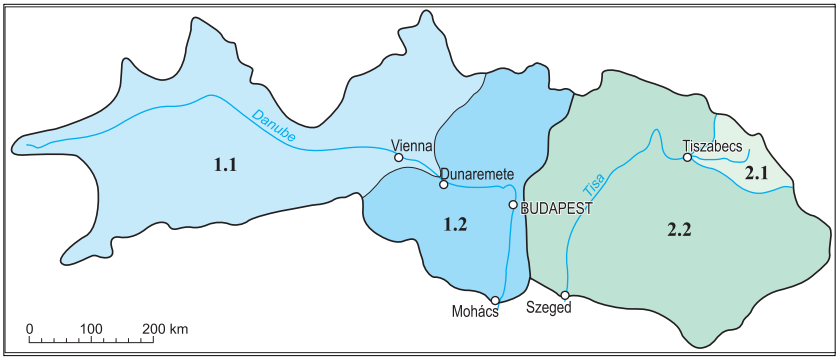

Fig. 1. The drainage basins of the Danube and the Tisza rivers. – 1.1 = the Danube catchment upstream of Dunaremete; 1.2 = the Danube catchment between Mohács and Dunaremete; 2.1 = the Tisza catchment above Tiszabecs; 2.2 = the Tisza catchment between Tiszabecs and Szeged

There is significant variation between the drainage basins of the two rivers. On the Danube catchment Alpine (high-mountain) climate, while in the northern Alpine foreland moist Atlantic climate is typical. Here the predominance of temperate maritime air masses deriving from the middle to high geographical latitudes of the Atlantic Ocean and of subtropical Atlantic maritime air masses is characteristic (Bacsó, N. 1959; Péczely, Gy. 1979). In the Tisza drainage basin, i.e. in the NE and E parts of the Carpathian Basin middle-mountain (dry continental) climate prevails. In the climate temperate continental air masses, primarily from Asia, and polar air masses are of significant importance. Thus, in the Alpine foreland the influence of maritime air masses, while in the NE and E parts of the Carpathian that of continental air masses are decisive. The paper investigates the impact of the climate of both catchments on the water temperature conditions. The 60-year observation series also allows the presentation of the hydrological impact of global warming.

Climatic character and water temperature

There is no significant difference between the *annual mean water temperature* of the two rivers when they enter Hungary: the Danube at Dunaremete has a value of 10.4 °C and the Tisza at Tiszabecs 10.0 °C. The annual and monthly

curve of water temperature for the rivers arriving from the 131,543 km² basin W of the Carpathian Basin and from the 9,707 km² basin in the NE-Carpathians reflects climatic variations less directly.

Minimum monthly water temperature is observed for both rivers in January: on the average the Danube at Dunaremete is warmer (2.3 °C) than the Tisza at Tiszabecs (0.7 °C). The values are influenced by mild Atlantic winters as opposed to longer continental winters *(Table 1).*

Table 1. Monthly and annual water temperatures of both rivers at the entrance to Hungary, 1951–2010, °C

Jan	Feb	Mar	Apr	May	Jun	Jul	Aug	Sep	Oct	Nov	Dec	Year
The Danube at Dunaremete, 131,543 km²												
2.3	3.0	5.6	9.6	13.5	16.7	17.9	18.1	15.7	11.8	7.3	3.7	10.4
The Tisza at Tiszabecs, 9,707 km²												
0.7	1.0	3.8	8.5	14.2	18.1	20.0	19.7	15.7	10.4	5.2	1.9	10.0

In the NE-Carpathians, to the influence of cold continental air masses, warming is more gradual than on the catchment to the W of the Carpathian Basin. As a consequence, *until April the water temperature of the Tisza is lower than that of the Danube*. In the summer period (from May to September) the warmer continental summer also contributes to the higher water temperature of the Tisza.

The *maximum monthly water temperatures* reflect the summer temperature conditions W and E of the Carpathian Basin, respectively., as the Danube at Dunaremete peaks 18.1 °C (in August) and the Tisza at Tiszabecs 20.0 °C (in July).

The range of the monthly mean temperatures is higher for the Tisza (19.3 °C) than for the Danube (15.8 °C). The differences in discharge are also influential in this respect (*Figure 2).* Heat energy arrives in similar amounts but the lower water mass of the Tisza warms up more rapidly and to greater extent.

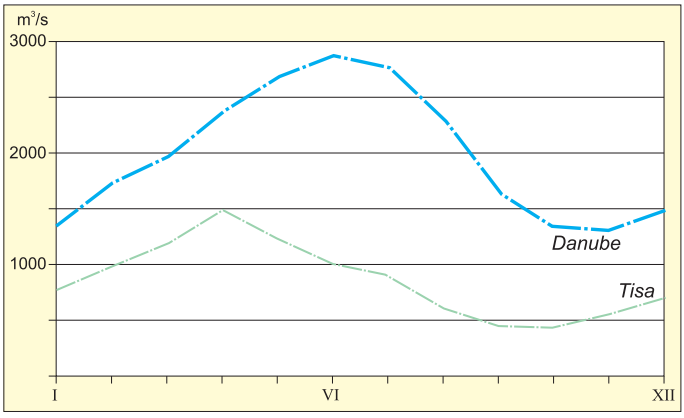

Fig. 2. The mean monthly discharges of the Danube and the Tisza, 1951–1980, m³/sec

Changes along the longitudinal profile of the Hungarian section

The length of the Hungarian section of the Danube is 378.6 km, while the Tisza is 51% longer (572.3 km). The growth of the Danube catchment area from Dunaremete to Mohács in the W margin of the Carpathian Basin is 77,521 km^2, while for the Tisza from Tiszabecs to Szeged in the NE and E part of the Carpathian Basin is 128,701 km^2 *(Figure 1*).

The climate of the E part of the Carpathian Basin is strongly influenced by the Carpathian ranges, which in winter moderate the effect of cold air masses generated over N-Asia, often modifying the direction of air currents (Péczely, Gy. 1979). The water temperature of the Tisza is remarkably influenced by the heat input from the tributaries on Hungarian territory and the temperature of inflow of communal and industrial sewage since the river transports only 36% (855 m^3/s) of the discharge of the Danube. These kinds of effects are less significant for the Danube. On the territory of Hungary the long-term mean temperature of the Danube rises by 1.2 °C and of the Tisza by 2.0 °C (*Table 2).*

Table 2. Changes in the monthly and annual mean temperatures of the Danube and Tisza in Hungary, 1951–2010, °C

Jan	Feb	Mar	Apr	May	Jun	Jul	Aug	Sep	Oct	Nov	Dec	Year
The Danube between Dunaremete and Mohács, 378.6 km												
-0.3	-0.1	0.1	1.0	2.0	12.1	2.7	2.7	1.9	1.2	0.5	-0.2	1.2
The Tisza between Tiszabecs and Szeged, 572.3 km												
0.2	0.5	0.8	2.1	2.5	2.9	3.0	3.2	3.1	3.0	2.0	0.7	2.0

In the winter months (from December to February), arriving from the Atlantic regions with mild winters to the continental Carpathian Basin, the Danube loses from its temperature. The same phenomenon does not apply for the Tisza as in the NE-Carpathians the continental winters are colder than in the E parts of the Carpathian Basin, where *the Carpathian Mountains often prevent the penetration of cold continental air masses from the direction of Siberia* (Péczely, Gy. 1979). As a result of the protective effect of the Carpathians the left-bank tributaries bring warmer water than those coming from the NE-Carpathians. The temperature difference between the two rivers is most pronounced in the summer and early autumn (between June and October). To the influence of the cold air masses arriving from easterly direction, after November the water of the Tisza cools more rapidly than the Danube *(Table 3).*

As a consequence of the temperature conditions of the Carpathian Basin, the Danube, which was warmer, when reached Hungary, is colder, when leaving the country, than the Tisza *(Table 1*).

Table 3. Monthly and annual water temperatures of both rivers leaving Hungary at the S border, 1951–2010, °C

Jan	Feb	Mar	Apr	May	Jun	Jul	Aug	Sep	Oct	Nov	Dec	Year
The Danube at Mohács, 209,064 km^2												
2.0	2.9	5.7	10.6	15.5	18.8	20.6	*20.8*	17.6	13.0	7.8	3.5	11.6
The Tisza at Szeged, 138,408 km^2												
0.9	1.5	4.6	10.6	16.7	21.0	*23.0*	22.9	18.8	13.4	7.2	2.6	12.0

The trends of water temperature change between 1951 and 2010

The trend of mean water temperature changes of both rivers is related to global warming (Mika, J. 1988, 1989, 1991; Bartholy, J. *et al.* 2007 and others). The temperature of waters flowing in from catchments lying W from the Carpathian Basin rises more rapidly than that of waters deriving from the E parts of the Basin *(Table 4*).

Table 4. Trend of change in annual mean temperature, 1951–2010, °C

Station	Area, km^2	Y[1]	Trend, °C/60 years
Mohács (Danube)	209,064	0.0243	1.46
Szeged (Tisza)	138,408	0.0149	0.89

[1] Coefficient of the regression equation

The general rising trends of variable extent are interrupted by short spells of positive and negative fluctuations, which primarily depend on winter and summer air temperatures *(Figure 3).* The trends of mean annual minimum (winter) and annual maximum (summer) temperatures represent most faithfully the impact of winters and summers on water temperature. Climate change is most remarkably manifested in the temperature and precipitation conditions of these seasons. The *waters in the coldest month of the year* arrive from the catchment of 131,543 km^2 area W of the Carpathian Basin with a positive trend of 2.31 °C/60 years, while waters from the NE-Carpathians show a very weak negative trend *(Table 5).*

The tendency of water temperature changes indicates that the impact of ever milder winters is not observed in the mountainous NE parts of the Carpathian Basin.

Table 5. Trend of changes in minimum monthly mean temperatures, 1951–2010, °C

Station	Area, km^2	Y[1]	Trend, °C/60 years
Dunaremete (Danube)	131,543	0.0385	2.31
Tiszabecs (Tisza)	9,707	-0.0042	-0.25

[1] Coefficient of the regression equation

In the hottest summer month the positive trend (1.28 °C/60 years) of waters from the Danube catchment W of the Carpathian Basin points to summers getting warmer at a slower pace than winters are getting milder (*Table 6).* In the NE-Carpathians summer temperatures virtually remain the same (trend: -0.03 °C/60 years).

Table 6. Trend of changes in maximum monthly mean temperatures, 1951–2010, °C

Station	Area, km²	Y[1]	Trend, °C/60 years
Dunaremete (Danube)	131,543	0.0213	1.28
Tiszabecs (Tisza)	9,707	-0.0005	-0.03

[1] Coefficient of the regression equation

The tendencies confirm that *the rise of winter temperatures in the catchment W of the Carpathian Basin is remarkable, while no change is observed in summer temperatures*. The trends observable along the Hungarian sections of both rivers also reflect the modifying effect of the climate of drainage basins to which the Carpathian Basin was added *(Figure 3).* The effect is manifested in the variation of the Y coefficient values.

In winter the most pronounced changes are found in the water temperature of the Tisza River. The 1.24 °C/60 years positive trend along the Hungarian section of 572.3 km length, between Tiszabecs and Szeged, indicates significant warming during winter in the E parts of the Carpathian Basin *(Table 7).* The Tisza arrives from a catchment of severe climate upstream of Tiszabecs into the Carpathian Basin, where winters are milder and river water temperature rises. The water temperature of the Danube reduces along its Hungarian section of 378.6 km length because the river flows from a W region of mild Atlantic winters into the relatively colder Carpathian Basin.

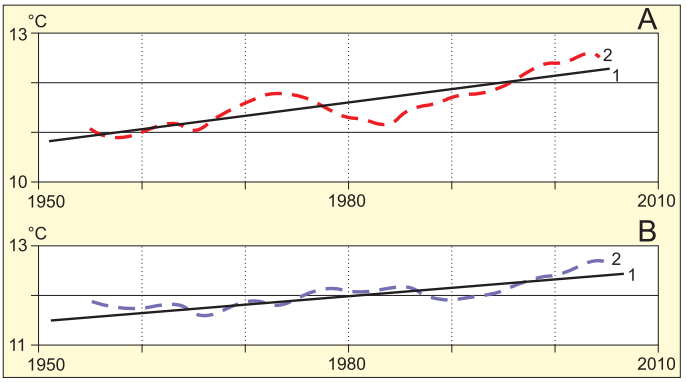

Fig. 3. Changes in the water temperatures of the Danube and the Tisza, 1951–2010, °C. – 1 = linear trend (regression line); 2 = moving trend (means for 10 values)

Table 7. Trend of changes in minimum monthly mean temperatures for the Hungarian sections of the Danube and the Tisza rivers, 1951–2010, °C

Station	Area, km^2	Y[1]	Trend, °C/60 years
Dunaremete (Danube)	131,543	0.0385	2.31
Mohács (Danube)	209,064	0.0208	1.25
Tiszabecs (Tisza)	9,707	-0.0042	-0.25
Szeged (Tisza)	138,408	0.0098	0.59

[1] Coefficient of the regression equation

The summer water temperatures show a much moderate rising trend (0.08 °C/60 years) for the Hungarian Danube section (378.6 km) between 1951 and 2010 than for the Hungarian Tisza section of 572.3 km length (1.1 °C/60 years) *(Table 8)*.

Table 8. Trend of changes in maximum monthly mean temperatures for the Hungarian sections of the Danube and the Tisza rivers, 1951–2010, °C

Station	Area, km^2	Y[1]	Trend, °C/60 years
Dunaremete (Danube)	131,543	0.0385	2.31
Mohács (Mohács)	209,064	0.0398	2.39
Tiszabecs (Tisza)	9,707	-0.0005	-0.03
Szeged (Tisza)	138,408	0.0179	1.07

[1] Coefficient of the regression equation

The more remarkable warming trend of the Tisza River is influenced by its course 192.7 km longer than that of the Danube and the fact that in summer the Tisza has 26 and 22% lower discharges than the Danube. The identical amount of heat warms the lower amount of water more efficiently.

The *singular positive and negative fluctuations* within the above outlined trends (*Figure 4*) are remarkable in the monthly changes of water temperatures for the Danube catchment upstream of Mohács (209,064 km^2 area) and for the Tisza catchment upstream of Szeged (138,048 km^2 area).

The tendency of ever milder winters is not continuous. Since the mid-1960s it is evident for approximately 10 years but then it is followed by almost stagnation (*Figure 4*, A). In the E part of the Carpathian Basin the weak negative trend is replaced by a weak positive trend of ca 15-year duration from the mid-1960s (*Figure 4*, B). Since the early 1980s there has been a very moderate rise to the present. *The singular changes in monthly mean water temperatures for the coldest winter months in the period 1951 to 2010 confirms that winters started to become ever milder in the region W of the Carpathian Basin in the early 1960s.*

Summer warming in the Danube catchment W of the Carpathian Basin only began in the beginning of the 1980s (*Figure 4*, C). A marked rise in temperatures has been continuing to our days. In the E part of the Carpathian Basin the remarkable positive trend also dates back to the beginning of the 1980s,

but this process is significantly slowing down since the early 1990s (*Figure 4*, D). *The singular changes in monthly mean water temperatures for the hottest summer months indicate that summers started to become hotter only in the early 1980s and in the region W of the Carpathian Basin this process has been more marked than in the E part of the Carpathian Basin*.

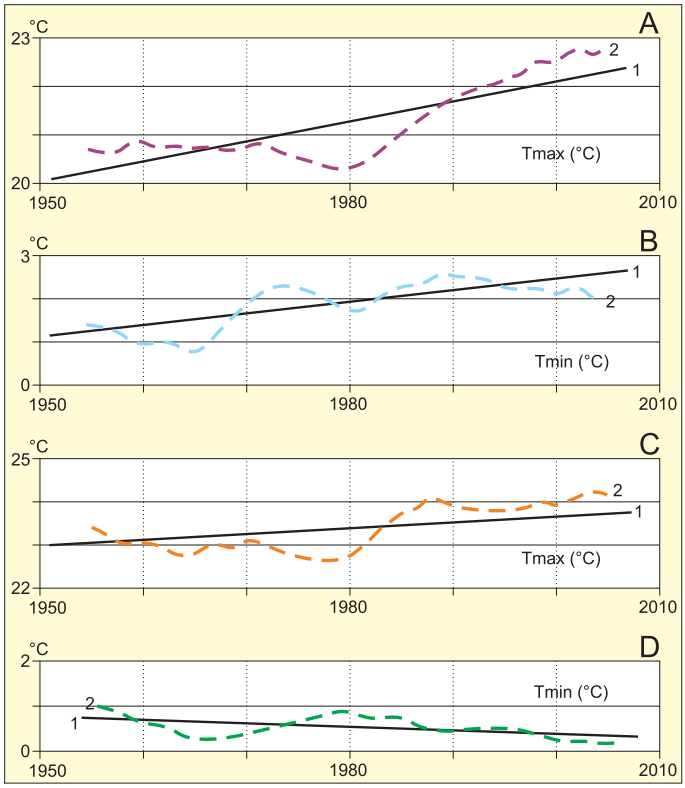

Fig. 4. Trend of changes of the coldest winter months (Tmin, °C) and of the warmest summer months (Tmax, °C), 1951–2010. – 1 = linear trend (regression line); 2 = moving trend (means for 10 values)

Conclusions

From the analyses of the 60-year long observation series the following conclusions can be drawn. In function of climate on the upstream catchment, the water of the Danube is generally warmer at the entrance to the Carpathian Basin than that of the Tisza, but in summer the Tisza water reaches higher temperatures and also its annual temperature range is higher. After November the water of the Tisza cools more rapidly than the Danube.

The overall rising trend in the monthly mean temperatures of Danube water indicate remarkable climate change, winters getting milder in the catchment section upstream of Dunaremete, while a similar trend cannot be pointed out for the Tisza catchment in the NE-Carpathians. These trends does not show steady warming but are interrupted by short spells of positive and negative fluctuations, which primarily depend on winter and summer air temperatures.

REFERENCES

Bacsó, N. 1959. *Magyarország éghajlata* (Climate of Hungary). Budapest, Akadémiai Kiadó, 302 p.

Bartholy, J., Pongrácz, R. and Pattantyús-Ábrahám, M. 2007. A cirkulációs viszonyok változásának elemzése az atlanti-európai térségben (Analysis of changes in air circulation in Atlantic Europe). *Légkör* 52. 18–24.

Greguss, Gy. 1866. A Dunavíz hőmérséklete vonatkozólag a hazai viszonyokra (Water temperature of the Danube in Hungary). *Matematikai és Természettudományi Közlemények* 4. Budapest, MTA, 472. p.

Lászlóffy, W. 1956. *Folyóink és tavaink hőmérsékleti viszonyai* (Temperature conditions of lakes and rivers in Hungary). Beszámoló a VITUKI 1955. évi kutatásairól. Budapest, VITUKI, 131–146.

Mika, J. 1988. A globális felmelegedés regionális hatásai a Kárpát-medencében (Regional impact of global warming in the Carpathian Basin). *Időjárás* 92. 178–189.

Mika, J. 1989. A globális felmelegedés és magyarországi hatásai (Impacts of global warming in Hungary). *Vízügyi Közlemények* 71. 542–599.

Mika, J. 1991. A nagyobb globális felmelegedés várható magyarországi sajátosságai (Predictable characteristics of major global warming in Hungary). *Időjárás* 95. 265–278.

Pasteiner, D. 1905. A Tisza folyó hőfoka (Temperature of the Tisza River). *Vízrajzi Évkönyv* 13. Budapest, Országos Vízépítési Igazgatóság, 141–150.

Péczely, Gy. 1979. *Éghajlattan* (Climatology). Budapest, Tankönyvkiadó, 336 p.

Hungary in Maps

Edited by
Károly Kocsis and Ferenc Schweitzer

Geographical Research Institute Hungarian Academy of Sciences
Budapest, 2009. 212 p.

'Hungary in Maps' is the latest volume in a series of atlases published by the Geographical Research Institute of the Hungarian Academy of Sciences. A unique publication, it combines the best features of the books and atlases that have been published in Hungary during the last decades. This work provides a clear, masterly and comprehensive overview of present-day Hungary by a distinguished team of contributors, presenting the results of research in the fields of geography, demography, economics, history, geophysics, geology, hydrology, meteorology, pedology and other earth sciences. The 172 lavish, full-colour maps and diagrams, along with 52 tables are complemented by clear, authoritative explanatory notes, revealing a fresh perspective on the anatomy of modern day Hungary. Although the emphasis is largely placed on contemporary Hungary, important sections are devoted to the historical development of the natural and human environment as well.

In its concentration and focus, this atlas was intended to act as Hungary's 'business card', as the country's résumé, to serve as an information resource for the sophisticated general reader and to inform the international scientific community about the foremost challenges facing Hungary today, both in a European context and on a global scale. Examples of such intriguing topics are: stability and change in the ethnic and state territory, natural hazards, earthquakes, urgent flood control and water management tasks, land degradation, the state of nature conservation, international environmental conflicts, the general population decline, ageing, the increase in unemployment, the Roma population at home and the situation of Hungarian minorities abroad, new trends in urban development, controversial economic and social consequences as a result of the transition to a market economy, privatisation, the massive influx of foreign direct investment, perspectives on the exploitation of mineral resources, problems in the energy supply and electricity generation, increasing spatial concentration focused on Budapest in the field of services (e.g. in banking, retail, transport and telecommunications networks), and finally the shaping of an internationally competitive tourism industry, thus making Hungary more attractive to visit.

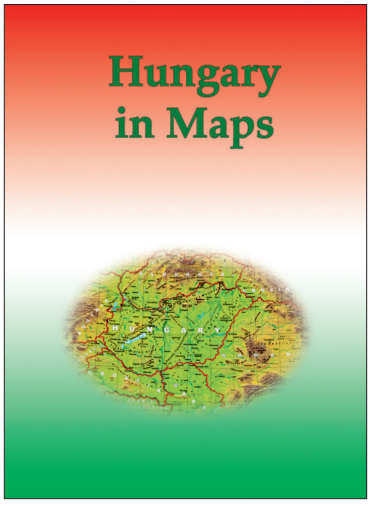

This project serves as a preliminary study for the new, 3rd edition of the National Atlas of Hungary, that is to be co-ordinated by the Geographical Research Institute of the Hungarian Academy of Sciences.

Price: EUR 20.00
Order: Geographical Institute RCAES HAS Library
H-1112 Budapest, Budaörsi út 45.
E-mail: magyar.arpad@csfk.mta.hu

Parallelization of Last Glacial loess-paleosol section of Red Hill with Heinrich events and ice core records

Éva KIS[1]

Abstract

In this paper, I would like to provide refined relative chronological data to loess-paleosol section situated on the IV. and V. terraces of Red Hill (Moravia), based on a comparison with Heirich events, North and South hemispheric ice core records. The last glacial–interglacial loess section is almost complete, all of the interstadial soils can be identified in the series instead of the eroded upper part of the PK I complex.

The onset of the formation of recent soil can be parallelized to H_0 event (~12 000), the double structural soils to H_1 and H_2 events, the eroded soils of PK I to H_3 and H_4, while the lower part of the complex has been correlated with H_5 and H_6 events (~63 ka BP). The loess series above PK I has been classified into Würm-3, the strata between PK I and PK II belong to the Würm-2. The lower part, under PK II is mostly clayey, cannot be regarded as a cold climate deposit. After the Riss/Würm interglacial the climate has changed slowly, and the typical glacial climate has started only after 75 ka BP.

Keywords: Heinrich events, ice cores, loess-paleosol series, chronology, $\delta^{18}O$ values

Introduction

Main aim of this paper is to provide new, refined relative chronological data on the formation of loess-paleosol deposits in Southern Moravia (*Photos 1–2*). The section is located on Devonian red sandstone and pebbles, and Miocene sandstone at the IV–V. terraces of the Red Hill (*Photo 3*). This investigation was based on records of Heinrich events, North and South hemispheric ice core drillings, and on the comparison of these paleoenvironmental proxies with our former loess-studies in the region (Kis, É. *et al.* 2011).

The stratigraphic investigations of the Red Hill section have been made by Kukla, G.J. (1975); Fink, J. and Kukla, G.J. (1977); Smolikova, L. (1982), Zeman, A. (1992) and Demek, J. *et al.* (2005). Loess deposits are important terres-

[1] Geographical Institute, Research Centre for Astronomy and Earth Sciences (Hungarian Academy of Sciences) H-1112 Budapest, Budaörsi út 45. E-mail: kis.eva@csfk.mta.hu

Photo 1. The South Czech "Red Hill" (Photo: Kıs, É.)

Photo 2. Perspective view of the terrace system of Red Hill (*source:* GoogleEarth™)

Photo 3. Devonian red sandstone and pebbles underlying the loess-paleosol section at the IV. terrace (Photo: Kis, É.)

trial archives of climatic changes (Lóczy, D. and Szalay, L. 1995; Lóczy, D. 2008) and these aeolian dust deposits provide insight into the Plio-Pleistocene geomorphological and environmental development of Central Europe (Frechen, M. *et al.* 1997, 2003; Fábián, Sz.Á. *et al.* 2004; Kovács, J. *et al.* 2011).

During the last glacial period, the dust transportation was defined by three prevailing wind-directions: (1) westerlies in the east-west corridor along latitude 50°N, (2) northwesterly winds from the Fennoscandinavian ice sheet, and (3) according to Rozycki, S.Z. (1991) and Rousseau, D.D. *et al.* (2007) the Saharan dust from south was also relevant. This last conception about the role of the Saharan dust was confirmed by the studies of Varga, Gy. (2011) and Varga, Gy. *et al.* (2012).

Methods

The sedimentary and stable isotopic parameters of the investigated, almost complete loess-paleosol section have been compared to the isotopic records of NGRIP (Greenland), EPICA Dome-C and Vostok (Antarctica) ice cores and to the North Atlantic Heinrich layers (*Figures 1–2*). I would like to correlate the

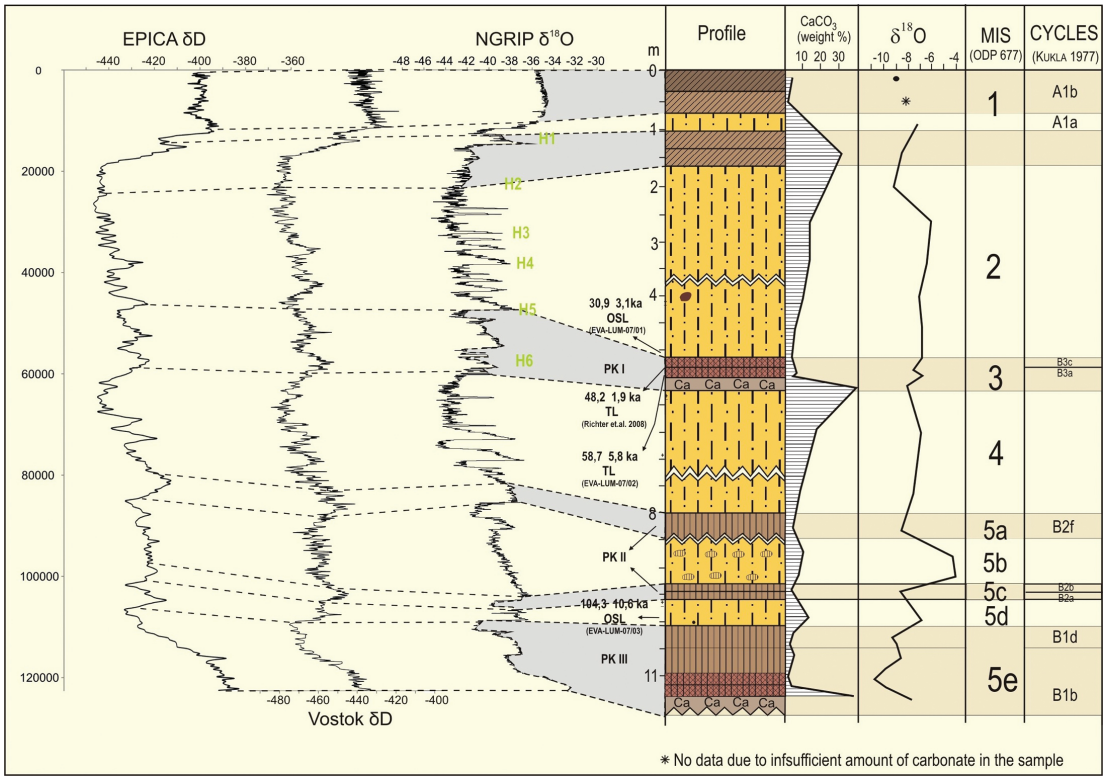

Fig. 1. Possible correlation of the last glacial/interglacial loess-paleosol series of the Red Hill with Heinrich events, Antarctic EPICA and Vostok δD, and Greenlandic NGRIP $\delta^{18}O$ records (Kis, É.). Sedimentary parameters: Kis, É. Stratigraphic analysis: Schweitzer, F., Kis, É., Balogh, J. and Di Gléria, M. Oxygen isotope measurements: Futó, I. and Vodila, G. Grain-size analysis: Di Gléria, M. (Data sources of ice core records and Heinrich events: Petit, J.R. *et al.* 1999; EPICA Community members 2004; NGRIP Community members 2004; Hemming, S.R. 2004)

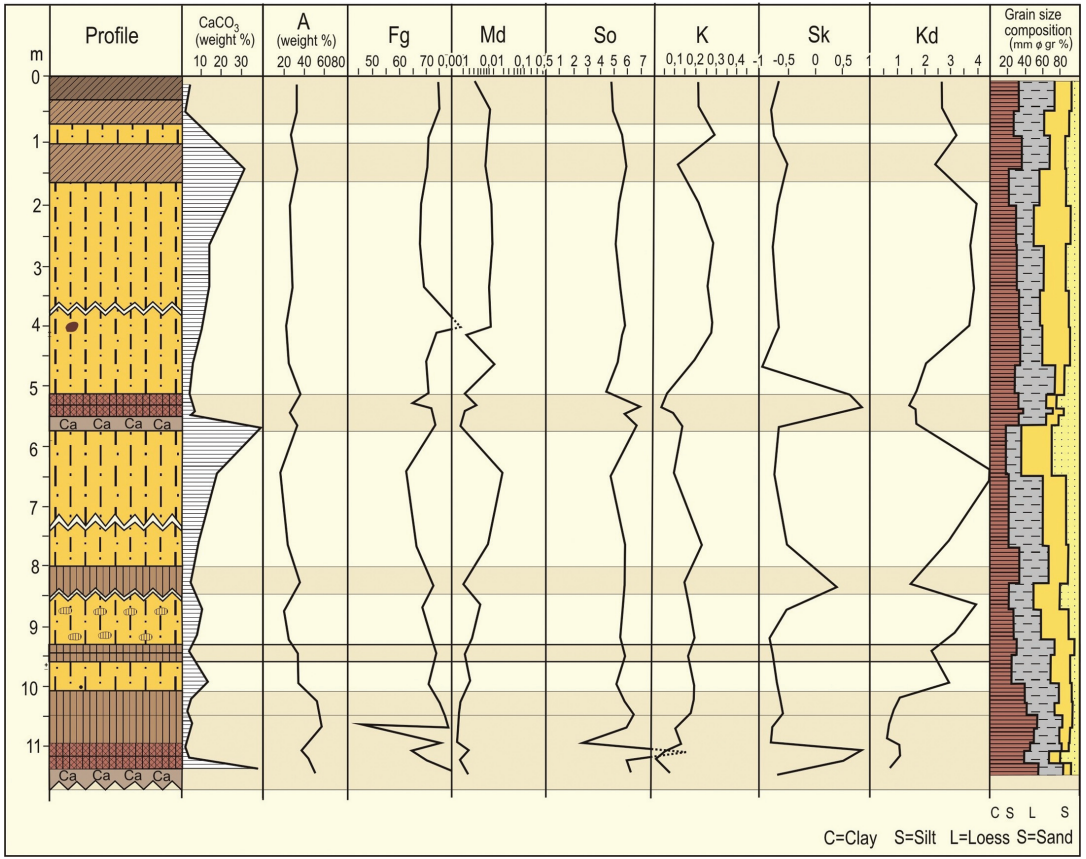

Fig. 2. Variations of sedimentary parameter values in the Red Hill loess-paleosol series (source: Kıs, É. *et al.* 2011). Sedimentary parameters: Kıs, É. Stratigraphic analysis: Schweitzer, F., Kıs, É., Balogh, J. and Di Gléria, M. Grain-size analysis: Di Gléria, M.

δD and $\delta^{18}O$ values of ice cores with the measured $\delta^{18}O$ values of the analysed loess-paleosol deposits to refine the chronological framework of the section.

The sedimentary parameters of the Red Hill section have been determined by environmental-discrimination proxies (Kıs, É. 2003; Schweitzer, F. and Kıs, É. 2003; Kıs, É. *et al.* 2011, 2012). These are traditional sedimentary parameters and our newly introduced indices (fineness grade: F_g and degree of weathering: K_d), and $\delta^{18}O$-values. The detailed description of the applied methods can be found in Kıs, É. *et al.* (2011).

The NGRIP ice core (Greenland)

The ice core provides information on the climatic changes and anomalies during the last glacial period of the North Atlantic domain (*Figure 1*). According to the North GRIP Community Members (2004), the analytical data represent 25 Dansgaard-Oeschger (D/O) events; abrupt, large amplitude climate fluctuations (often within several decades).

These events show us the rapid changes of cold and warm periods of the region. The D/O events can be correlated well with other North Atlantic paleotemperature proxies (e.g. benthic foraminiferal isotope records of VM23-0.81, DSDP 609, VM30-101k deep sea cores – Bond, G.C. *et al.* 1993; Ziegler, M. *et al.* 2008) or with terrestrial aeolian dust deposits (Varga, Gy. 2010). The stable isotope values and gas content of ice cores suggest the occurrence of abrupt 8–16°C temperature fluctuations during the last glacial period.

EPICA Dome Concordia (DOME C) ice core (Antarctica)

The EPICA DOME C ice core contains information on the climate changes of the last 800 kyr, the only one ice core which could have provide climate data on cyclic changes from the Brunhes/Matuyama Boundary (*Figure 1*). Beside the stable isotopes, the greenhouse gas content trapped in bubbles can be used as proxy of climatic fluctuations. Based on the detailed analyses of the sequence, eight glacials and interglacials (and their durations) have been distinguished during the last 800 kyr. Earlier Antarctic ice cores provide data only on the climate of the last 400 kyr (e.g. Vostok – Petit, J.R. *et al.* 1999).

The ice core records can be correlated with the benthic foraminiferal records and $\delta^{18}O$ values of deep sea deposits (e.g. ODP 659 Tiedemann, R. *et al.* 1994; Lisiecki, L. and Raymo, M.E. 2005), confirming the eight glacial cycles of the last 800 kyr.

Vostok ice core (Antarctica)

The more than 3700 metres deep ice core represent the climatic cycles of the last 440 kyr (*Figure 1*). (The third deepest lake of the Earth, Lake Vostok subglacial lake can be found beneath the Vostok Station.) Various measurements provide data on local paleotemperature, humidity, wind speed, atmospheric O_2, CO_2 and CH_4 content, lithic material of ancient volcanic eruptions. Based on the correlation of δD values of the ice core with $\delta^{18}O$ values of GRIP core (Jouzel, J. *et al.* 1997), all of the 25 D/O events of the last glacial periods can be found in the sequence. However, the relationship between the two regions is asynchronous; the warming phases had been occurring earlier in the Vostok cores compared to the Greenland ice cores. The northern ice cores have ~1,500 years lag behind the southern hemispheric climatic variations, but the global changes can be well correlated with statistical analyses of the phase-lag relationships.

Oxygen isotope values of the ice cores

Dansgaard, W. has established that the isotope ratio of $H_2{}^{18}O/H_2{}^{16}O$ of precipitation is constantly decreasing into the direction of higher latitudes, implying a strong relationship between temperature and stable isotope content. The temporal changes of isotopic composition of the precipitation provide information on the temperature changes. This relationship can be used to determine the paleotemperature from the ice cores oxygen isotope values. The values have been different during glacial and interglacial periods (Dansgaard, W. *et al.* 1983).

Oeschger, H. measured similar differences between cold and warm phases in the sequence of the Grenzensee deposits in Switzerland (Dansgaard, W. *et al.* 1993). These climatic fluctuations are not only typical for Greenland and Switzerland, however represent the whole northern hemispheric changes. The early measurements were confirmed by the recent NGRIP drillings and measurements (NGRIP Community Members 2004). The abrupt warming episodes and the longer cooling phases have determined the last glacial period.

Heinrich events

Heinrich events provide valuable information to recognition of paleoenvironmental, paleoclimatic and principally global climate changes. These events caused relatively rapid changes on a global paleoclimatic temporal scale. To recognize the causes of climate changes, the complex effects of terrestrial,

oceanic and atmospheric components should be investigated together. The deep sea deposits and ice cores provide the most comprehensive and complex picture on climate changes. These proxies reflect the variability of climatic stages and the variations of components on various temporal scales, even the seasonal changes. Heinrich events correlate with the destruction of the Arctic ice-sheets, and with the consequent release of vast volume of icebergs to North Atlantic. Signs of the events can be observed in the deep sea deposits after periodic major, mainly longer cold episodes.

These last glacial events were first reported by Heinrich, H. (1988) and by Bond, G.C. *et al.* (1992). The deep sea sediments of North Atlantic consist several layers rich in ice rafted terrestrial material and with decreased foraminiferal abundance. These, so called Heinrich layers can be correlated with cooling periods of marine and terrestrial environments, and also with decreased oceanic salinity. Investigations have confirmed that the cooling events can be connected to the presence and drifting of freshwater reservoir icebergs even at lower latitudes. The trails of the icebergs could be tracked trough 3000 km, following the melted detrital carbonate deposits. The deep sea sediments prove the abrupt cooling episodes in the last glacial period and the presence of vast volume of drifting icebergs.

Heinrich layers provide important sedimentary information on the short term, abrupt climate fluctuations by the repeated occurrence of ice rafted debris. The terrestrial material was eroded by glaciers and the calving icebergs transported it to the Atlantic Ocean. The melting and drifting icebergs dropped the embedded material onto the sea floor. The freshwater content of melted ice has changed significantly the oceanic and atmospheric circulation patterns.

Based on deep sea drillings, the Heinrich events were dated as the following: H_0: ~12 ka (Hemming, S.R. 2004); H_1: ~16.8 ka (Hemming, S.R. 2004), ~14 ka (Vidal, L. *et al.* 1999); H_2: ~24 ka (Hemming, S.R. 2004), ~22 ka (Bond, G.C. and Lotti, R. 1995; Vidal, L. *et al.* 1999); H_3: ~31 ka (Hemming, S.R. 2004), ~29 ka (Bond, G.C. and Lotti, R. 1995); H_4: ~38 ka (Hemming, S.R. 2004), ~37 ka (Bond, G.C. and Lotti, R. 1995), ~35 ka (Vidal, L. *et al.* 1999); H_5: ~45 ka (Hemming, S.R. 2004; Vidal, L. *et al.* 1999); H_6: ~60 ka (*Figure 1*).

The orientation of the H_1, H_2, H_4 and H_5 layers on the sea floor is north-south (from Labrador Sea into southern direction), while H_3 and H_6 deposits has west-east orientation (from North America into the direction of Europe, around the 40° northern latitude).

The main causes of Heinrich events are still a matter of scientific debate and there are several competing explanations about the processes leading to abrupt climatic fluctuations. The calving icebergs of the Laurentide ice sheet and the huge freshwater input could have major effect on the thermohaline circulation of the ocean, and causing southward (and westward) migration of North Atlantic Current. Consequently, the northward heat transport de-

creases, leading to the increase of Laurentide ice sheet. According to the EPICA Community Members (2004), the main causes can be traced back to changes of greenhouse gas concentration of the atmosphere. Even small-scale fluctuations of oceanic circulations (especially at Arctic regions) have major impact on the atmospheric CO_2 concentrations. The most important reservoir of CO_2 is the ocean, where fiftyfold of the atmospheric CO_2 can be stored. (The natural CO_2 concentration of the atmosphere was 200 ppm during the cold and 280ppm during the warm episodes).

Other investigations suggest various explanations on the causes; e.g. instability of West Arctic ice sheet; intensifying iceberg calving after cold winters; collapses of ice sheets due to backward erosion (Tiedemann, R. *et al.* 1994). The abrupt and large sea-level rises could have eroded the ice sheets leading to collapses. These explanations were also confirmed by model calculations (Arz, H.W. *et al.* 2007).

Generally, the Heinrich events occurred after a longer (7–10 kyr) cold period, which was terminated a massive release of calving and drifting icebergs. The H-events have been followed by an abrupt warming climatic phase. These cold-warm fluctuations of oceanic-atmospheric system between 20 and 80 ka BP were confirmed by the pioneering works of Bond, G.C. *et al.* (1993). Typical global environmental consequences of the Heinrich events are: decreased $\delta^{18}O$ content of deep sea deposits and decreased oceanic salinity related to the colder climate and to the increased influx of freshwater; increased grain-size of loess deposits indicating stronger winds due to the changing patterns of oceanic currents; increased sedimentation rate of lithic terrestrial fragments at the sea floor; palynological records show the replacement of oak by pines; and decreased foraminiferal abundance.

Results

This research is dealing with the last glacial period's (~100 kyr) stratigraphic features in a South Czech loess-paleosol section. I would like to compare the almost complete series of Moravian aeolian dust deposits to North and South hemispheric ice core records, Heinrich events and sea level changes. The aim of this paper is to complete the chronological framework of the investigated strata, based on the data contributed by Kis, É. *et al.* (2011).

The newest ice core and deep sea drillings provide new insight into dynamics of Plio-Pleistocene paleoenvironmental and paleoclimatic changes. These new databases of ice cores and deep sea sediments allow us to correlate the climatic fluctuations and the terrestrial, oceanic and atmospheric relationships with various proxies from different environments (e.g. loess deposits). In this case, the almost complete South Czech "Red

Hill" loess-paleosol sequence has been compared with the last glacial oscillations. With this comparison, the main aim is to refine the chronological properties of the section. The known intensity, duration and absolute age data of deep sea Heinrich events provide ground for relative dating and correlation of the investigated deposits. Based on these parallelization, the controversial stratigraphic position and ^{14}C data of thin, humic horizons above (and between) thick, well-developed paleosoils (e.g. in the Hungarian Tápiósüly–Dunaújváros loess series) can also be explained. The sedimentary parameters and oxygen isotope data of the series have been used during this comparison.

The investigated 120–130 kyr comprise the paleoenvironmental properties of the last glacial and interglacial periods. During the last interglacial the arctic summers were warmer by 5°C than the later epochs. All of the glaciers have been melted, only the inner part of Greenland remained covered by ice. As a result of the huge amount of melted ice, the sea level has been increased by 5 metres. The temperature of the last glacial maximum (21 ka BP) was colder by 20°C than present conditions (Miler, G.H. *et al.* 2010). The Heinrich events had various intensity and duration. Based on the deep sea records, the H_3 and H_6 events were fairly different than the others; the spatial distribution of the ice-rafted debris of these events is also different.

The investigated section consist of loess and intercalated soils of the last 100 kyr, however the lower part (between 100 and 80 ka BP) cannot be regarded as typical loess, these layers are sandy loess deposits (*Figure 1.; Photos 1 and 4–6.*). The loess section is generally intercalated by interstadial soils instead of the PK III., which is the last interglacial soil-series. The uppermost pedogenic complex consists of the recent (upper) and a redeposited paleosoil (lower). The onset of the soil-formation can be dated from 12 ka BP (preboreal oscillation), the preceding colder period is represented by the underlying loess layer.

The next thick soil is a double, weakly developed humic soil or structural paleosoil and can be correlated with the H_1 and H_2 events. The age of the upper pedogenic horizon is ~16.8 ka BP (Hemming, S.R. 2004), similarly to other loess sections in Central Europe (e.g. Paks: 16730±400 years; Dolní Vestonice). Loess between the two soil horizons cannot be found at the Red Hill, it was eroded or redeposited. The lower structural soil has been formed ~22–24 ka BP.

The thick Würm-3 loess series (*Photo 4*) represents well the cold glacial climate; while the upper part of the underlying PK I soil-complex is eroded. These missing horizons could be parallelized to the H_3 and H_4 events. The middle part of the PK I complex is related to the H_5 and H_6 events, the ages of these events are 45 and 60 ka BP (Vidal, L. *et al.* 1999; Hemming, S.R. 2004). The hiatus at the top of PK I is ~10 kyr.

Photo 4. Würm-3 loess series in the upper part of the section (Photo: Kıs, É.)

Similarly to Dolní Vestonice, the Würm-2 loess stratum is well-developed and fairly thick. Beneath the PK II soil-complex the section shows us that the climate has changed slowly after the last interglacial, the Würm-1 period was not a real cold stadial and cannot identified in the loess series; the temperature has decreased and the typical steppe environment was formed slowly.

This interpretation of the Red Hill loess section could also be confirmed by several evidences from the discussed ice core and deep sea records (*Figure 1*).

Photo 5. Periglacial features in young loess (Photo: Kıs, É.)

Photo 6. The PK I soil series with notable hiatus in the upper part (Photo: Kıs, É.)

REFERENCES

Arz, H.W., Lamy, F., Ganopolski, A., Nowaczyk, N. and Pätzold, J. 2007. Dominant Northern Hemisphere climate control over millennial-scale glacial sea-level variability. *Quaternary Science Reviews* 26. 312–321.

Bond, G., Broecker, W., Johnson, S., McManus, J., Labeyrie, L., Jouzel, J. and Bonani, G. 1993. Correlation between climate records from North Atlantic sediments and Greenland ice. *Nature* 365. 507–508.

Bond, G., Heinrich, H., Broecker,W., Labeyrie, L., McManus, J., Andrews, J., Huon, S., Jantschik, R., Clasen, S., Simet, C., Tedesco, K., Klas, M., Bonani, G. and Ivy, S. 1992. Evidence for massive discharges of icebergs into the North Atlantic ocean during the last glacial period. *Nature* 360. 245–249.

Bond, G.C. and Lotti, R. 1995. Iceberg discharges into the North Atlantic on millennial time scales during the last glaciation. *Science* 267. 1005–1010.

Dansgaard, W., Johnsen, S.J., Clausen, H.B., Dahl-Jensen, D., Gundestrup, N.S., Hammer, C.U., Hvidberg, C.S., Steffensen, J.P., Sveinbjörnsdottir, A.E., Jouzel, J. and Bond, G. 1993. Evidence for general instability of past climate from a 250-kyr ice-core record. *Nature* 364. 218–220.

Dansgaard, W., Oeschger, H. and Langway, C.C., Jr. 1983. Ice core indications of abrubt climate changes. In *Palaeoclimatic Research and Models*. Proceedings of Workshop, Brussels, Dec. 1982. Dordrecht–Boston–Lancaster, D. Reidel Publishing Company, 72–73.

Demek, J., Havliček, M., Kirchner, K., Nehyba, S., Petrová, P., Bubík, M. and Gilíkova, H. 2005. *Příspěvek k poznání geologické situace na JV svahu Červeného kopce v Brně.* Brno, Geol. výzk. Mor. Slez. v. r. Brno, 162 p.

EPICA community members, 2004. Eight glacial cycles from an Antarctic ice core. *Nature* 429. 623–628.

Fábián, Sz.Á., Kovács, J., Nagyváradi, L. and Varga, G. 2004. Was There Desert Climate in the Carpathian Basin, or Not? *Studia Geomorphologica Carpatho Balcanica* 38. 49–58.

Fink, J. and Kukla, G.J. 1977. Pleistocene climate in Central Europe at least 17 interglacials after Olduvai event. *Quaternary Research* 7. 363–371.

Frechen, M., Horváth, E. and Gábris, Gy. 1997. Geochronology of Middle and Upper Pleistocene loess sections in Hungary. *Quaternary Research* 48. (3): 391–312.

Frechen, M., Oches, E.A. and Kohfeld, K.E. 2003. Loess in Europe – mass accumulation rates during the Last Glacial Period. *Quaternary Science Reviews* 22. (18–19): 1835–1857.

Heinrich, H., 1988. Origin and consequences of cyclic ice rafting in the northeast Atlantic Ocean during the past 130,000 years. *Quaternary Research* 29. 142–152.

Hemming, S.R., 2004. Heinrich Events: Massive Late Pleistocene detritus layers of the North Atlantic and their global climate imprint. *Reviews in Geophysics* 42. 1–43.

Jouzel, J., Froehlich, K. and Schotterer, U. 1997. Deuterium and oxygen-18 in present-day precipitation: data and modelling. *Hydrological Sciences* 42. (5): 747–763.

Kis, É. 2003. The sequence of the Susak loess profile. In *Susak – environmental reconstruction of a loess island in the Adriatic*. Eds. Bognár, A., Schweitzer, F. and Szöőr, Gy. Budapest, Geographical Research Institute HAS, 51–66.

Kis, É., Schweitzer, F., Palcsu, L., Futó, I., Balogh, J. and Di Gléria, M. 2012. Investigations of paleogeographic variations on the basis of the stratotype section of Viatovo at the Lower Danube. *Hungarian Geographical Bulletin / Földrajzi Értesítő* 61. (2): 93–111.

Kis, É., Schweitzer, F., Vodila, G., Futó, I., Balogh, J. and di Gléria, M. 2011. Special paleogeographic characteristics of environs of the Moravian Plateau. *Hungarian Geographical Bulletin* 60 (3): 247–259.

Kovács, J., Fábián, Sz.Á., Varga, G., Újvári, G., Varga, Gy. and Dezső, J. 2011. Plio-Pleistocene red clay deposits in the Pannonian Basin: A review. *Quaternary International* 240. (1–2): 35–43.

Kukla, G.J. 1975. Loess stratigraphy of Central Europe. In *After the Australopithecines.* Eds. Butzer, K.W. and Isaac, G.L. The Hague–Paris, Mouton Publishers, 99–188.

Lisiecki, L. and Raymo, M.E. 2005. A Pliocene–Pleistocene stack of 57 globally distributed benthic $\delta^{18}O$ records. *Paleoceanography* 20. PA1003. 17 p.

Lóczy, D. 2008. A löszvidékek formakincse (Geomorphology of loess terrains). In *Geomorfológia II. Földfelszíni folyamatok és formák.* Ed. Lóczy, D. Budapest–Pécs, Dialóg Campus Kiadó, 55–58.

Lóczy, D. and Szalay, L. 1995. Assessment of loess as parent material for agro-ecological potential. *GeoJournal* 36. (2–3): 275–280.

Miller, G.H., Brigham-Grette, J., Alley, R.B., Anderson, L., Bauch, H.A., Douglas, M.S.V., Edwards, M.E., Elias, S.A., Finney, B.P., Fitzpatrick, J.J., Funder, S.V., Herbert, T.D., Hinzman, L.D., Kaufman, D.S., MacDonald, G.M., Polyak, L., Robock, A., Serreze, M.C., Smol, J.P., Spielhagen, R., White, J.W.C., Wolfe, A.P., and Wolff, E.W. 2010. Temperature and precipitation history of the Arctic. *Quaternary Science Reviews* 29. (15–16): 1679–1715.

North Greenland Ice Core Project members, 2004. High-resolution record of Northern Hemisphere climate extending into the last interglacial period. *Nature* 431. 147–151.

Petit, J.R., Jouzel, J., Raynaud, D., Barkov, N.I., Barnola, J.M., Basile, I., Bender, M., Chappellaz, J., Davis, J., Delaygue, G., Delmotte, M., Kotlyakov, V.M., Legrand, M., Lipenkov, V., Lorius, C., Pépin, L., Ritz, C., Saltzman, E. and Stievenard, M. 1999. Climate and Atmospheric History of the Past 420,000 years from the Vostok Ice Core, Antarctica. *Nature* 399. 429–436.

Richter, D., Tostevin, G., Skrdla, P. and Davies, W. 2009. New radiometric ages for the Early Upper Paleolithic type locallity of Brno-Bohunice (Czech Republic): comparison of OSL, IRSL, TL and ^{14}C dating results. *Journal of Archeological Science* 36. 708–720.

Rousseau, D.D., Derbyshire, E., Antoine, P. and Hatte, C. 2007. Loess records. Europa. Elsevier: 1440–1457.

Rozycki, Sz. 1991. *Loess and loess-like deposits*. Wroclaw, Ossolineum, Polish Acadamy of Sciences. 187 p.

Schweitzer, F. and Kis, É. 2003. Formation of loess and loess-like sediments. In *Susak – environmental reconstruction of a loess island in the Adriatic.* Eds. Bognár, A., Schweitzer, F. and Szöőr, Gy. Budapest, Geographical Research Institute HAS, 45–65.

Smolíková, L. and Zeman, A. 1982. Bedeutung der Ferretto-Böden für die Quartärstratigraphie. Praha, *Sbor. geol. věd. Antropozoikum* 14. 57–93.

Tiedemann, R., Sarnthein, M. and Shackleton, N.J. 1994. Astronomic timescale for the Pliocene Atlantic $\delta^{18}O$ and dust flux records of Ocean Drilling Program Site 659. *Paleoceanography* 9. (4): 619–638.

Varga, Gy. 2010. Gondolatok a porviharok és a klimatikus, környezeti folyamatok összefüggéseiről. (On the relationships between duststorms and climatic processes.) *Földrajzi Közlemények* 134. (1): 1–14.

Varga, Gy. 2011. Similarities among the Plio-Pleistocene terrestrial aeolian dust depositsinthe world and in Hungary. *Quaternary International* 234. (1–2): 98–108.

Varga, Gy., Kovács, J. and Újvári, G. 2012. Late Pleistocene variations of the background aeolian dust concentration in the Carpathian Basin: an estimate using decomposition of grain-size distribution curves of loess deposits. *Netherlands Journal of Geosciences – Geologie en Mijnbouw* 91. (1–2): 159–171.

Vidal, L., Schneider, R.R., Marchal, O., Bickert, T., Stocker, T.F. and Wefer, G. 1999. Link between the North and South Atlantic during the Heinrich events of the last glacial period. *Climate Dynamics* 15. 909–919.

Zeman, A. 1992. New data on the Quaternary at Červený kopec Hill in Brno. *Scripta, Geology* 22. 123–131.

Ziegler, M., Nürnberg, D., Karas, C., Tiedemann, R. and Lourens, L.J. 2008. Persistent summer expansion of the Atlantic Warm Pool during glacial abrupt cold events. *Nature Geoscience* 1. 601–605.

AVAILABLE!

Ethnic map of Hungary 1941 + Ethnic map of present territory of Hungary 2001

Scale 1:500 000

Authors: KOCSIS, K. and BOTTLIK, ZS.

Geographical Research Institute, Hungarian Academy of Sciences, Budapest, 2009

The latest (eighth) piece of ethnic map series of the Carpathian Basin was an attempt to draft the changes that have taken place in the ethnic structure during the past five hundred years as well as to display its present state with the help of ethnic maps and a chart - in our case referring to the present-day territory of Hungary. On the front pages of our work consisting of two sheets ethnic maps of the present-day territory of Hungary are displayed with the help of pie-charts, based on ethnic (2001) and mother tongue (1941) data. Population-proportional pie-charts provide information on the territorial distribution of the major ethnic groups and on the contemporary administrative division.

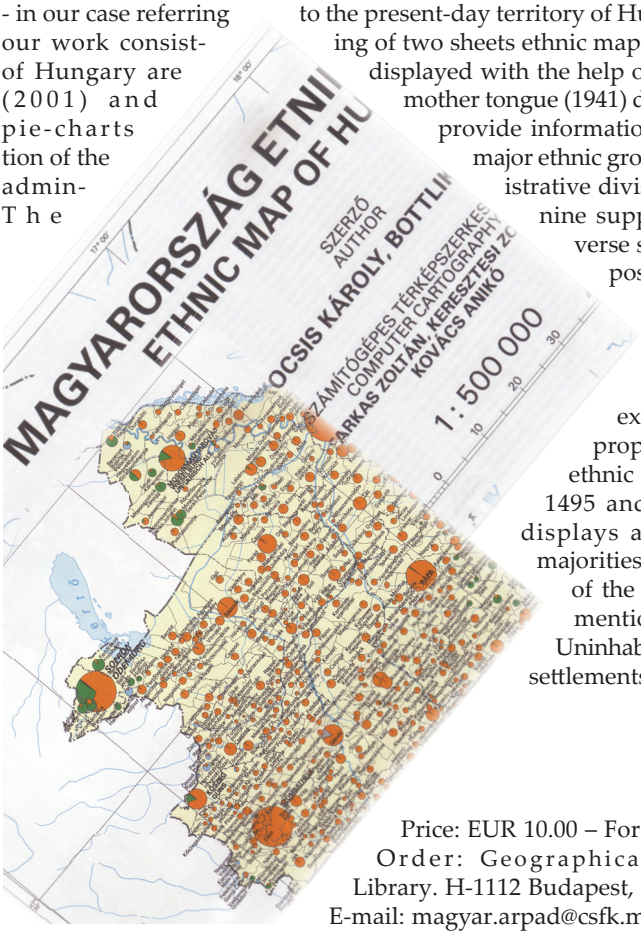

The nine supplementary maps on the reverse show the lingual-ethnic composition of the present-day territory of Hungary in 1495, 1715, 1784, 1880, 1910, 1930, 1941, 1990 and 2001 respectively. The chart here explores the quantitative and proportional changes of the main ethnic groups' population between 1495 and 2001. The series of maps displays absolute or relative ethnic majorities only in the inhabited areas of the settlements which had been mentioned in the source referred. Uninhabited areas with no permanent settlements are shown as blank spots.

Price: EUR 10.00 – For sale only in pairs!

Order: Geographical Institute RCAES HAS Library. H-1112 Budapest, Budaörsi út 45.
E-mail: magyar.arpad@csfk.mta.hu

Hungarian Geographical Bulletin 61 (4) (2012) pp. 343–348.

OECD Environmental Outlook to 2050. The Consequences of Inaction. Organisation for Economic Co-operation and Development, 2012, Paris, 349 p.

This book provides a detailed analyses of main economic, social and environmental trends for the world to 2050, and simulations of policy actions to address the key future challenges. Obviously humankind has witnessed unprecedented growth and prosperity in the last four decades, with the size of the world economy more than tripling and population increasing by over 3 billion people since 1970. This tremendous economic and population growth, however, has been accompanied by serious environmental degradation and natural resource depletion. The current growth model and the unsustainable use of natural resources could ultimately undermine future human development.

The authors of this *Outlook* ask "What will the next four decades bring for the world?" Based on joint modelling by the OECD and the NEAA (Netherlands Environmental Assessment Agency) it looks forward to the year 2050 to find out what demographic and economic trends might affect the environment if the mankind does not adopt more ambitious green policies and technologies. It also looks at what policies could change that picture for the better future of the next generations. This publication focuses on four areas: climate change, biodiversity, water and health impacts of pollution. These key environmental challenges were identified by the previous outlook to 2030 (OECD, 2008) as *Red Light issues* requiring urgent attention and decisive actions.

By 2050, the Earth's population is expected to increase from 7 billion to over 9 billion and the world economy is projected to nearly quadruple, with growing demand for energy and natural resources. Average GDP growth rates are projected to slow in China and India.

Nearly 70% of the world population is projected to be urban residents in 40 years time, magnifying challenges such as air pollution, transport congestion, and waste management. A

world economy four times larger than today is projected to use 80% more energy in 2050. Without more effective policies, the share of fossil energy in the global energy mix will still remain at about 85%. The emerging economies of the BRIICS states (Brazil, Russia, India, Indonesia, China and South Africa) are projected to become major energy users.

More disruptive climate change is likely to be locked in, with global greenhouse gas (GHG) emissions projected to increase by 50%, primarily due to a 70% growth in energy-related CO_2 emissions. (As a result, the global average temperature increase is projected to be 3°C to 6°C higher by the end of the century, exceeding the internationally agreed goal of limiting it to 2°C above pre-industrial levels. Surpassing the 2°C threshold would alter precipitation patterns, increase glacier and permafrost melt, drive sea-level rise, and worsen the intensity and frequency of extreme weather events. This will hamper the ability of people and ecosystems to adapt to increasing extreme situations.

Biodiversity loss is projected to continue, especially in Asia, Europe and Southern Africa. Globally, terrestrial biodiversity (measured as mean species abundance – or MSA – an indicator of the intactness of a natural ecosystem) is projected to decrease a further 10% by 2050. Primary forests, which are rich in biodiversity, are projected to shrink in area by 13%. The main pressures driving biodiversity loss include land-use change (*e.g.* agriculture), the expansion of commercial forestry, infrastructure development, urban sprawl, human encroachment and fragmentation of natural habitats, as well as pollution and climate change.

Freshwater resources availability will be further strained, with 2.3 billion more people than today (in total over 40% of the global population) projected to be living in river basins experiencing severe water scarcity, especially in North and South Africa, and South and Central Asia.

Global water demand is projected to increase by some 55%. Groundwater depletion may become the greatest threat to agriculture and urban water supplies in several regions. Nutrient pollution from urban wastewater and agriculture is projected to worsen in most regions, intensifying eutrophisation and damaging aquatic biodiversity. The Millennium Development Goals for sanitation will not be met by 2015; by 2050 1.4 billion people are projected to live still without access to basic sanitation facilities.

Air pollution is set to become the world's top environmental cause of premature mortality under this scenario**.** Air pollution concentrations in some cities, particularly in Asia, already far exceed World Health Organization safe levels. By 2050, the number of premature deaths from exposure to particulate matter is projected to more than double to reach 3.6 million a year globally, with most deaths occurring in China and India. The burden of disease related to exposure to hazardous chemicals is significant worldwide, but more severe in non-OECD countries where chemical safety measures are still insufficient.

These *Baseline projections* highlight the need for urgent action today to change the course of our future development. Natural systems have "tipping points" beyond which damaging change becomes irreversible (e.g. species loss, climate change, groundwater depletion, land degradation).

Acting now is environmentally *and* economically rational. Well-designed policies can reverse the trends projected in the *Outlook Baseline* scenario**.** Making reform happen will depend on political leadership and widespread public support that changes are both necessary and affordable. Not all of the solutions will be cheap, which is why seeking out the most cost-effective among them is so important. A key task is to improve understanding of the challenges and trade-offs that need to be made.

Integrating environmental objectives in economic and sectoral policies (e.g. energy, agriculture, transport) is vital, as the latter have greater impacts than environmental

policies alone. Environmental challenges should be assessed in the context of other global challenges such as food and energy security and poverty reduction. As many of the environmental problems are global in nature (e.g. biodiversity loss, climate change) or linked to the trans-boundary effects of globalisation, international co-operation is indispensable to ensure an equitable sharing of the cost of necessary measures.

The *OECD Environmental Outlook to 2050* with its very rich analytical background provides policy-makers, researchers and interested readers with guidance how to address more complex and long-term global environmental challenges and to enhance preventive, effective and efficient environmental policies for better and cleaner future of our children and grandchildren.

István Pomázi

Rátz, T. and Irimiás, A. eds.: Risk and Uncertainty in Tourism: Theory and Practice. Kodolányi János University of Applied Sciences, Székesfehérvár, 2012. 146 p.

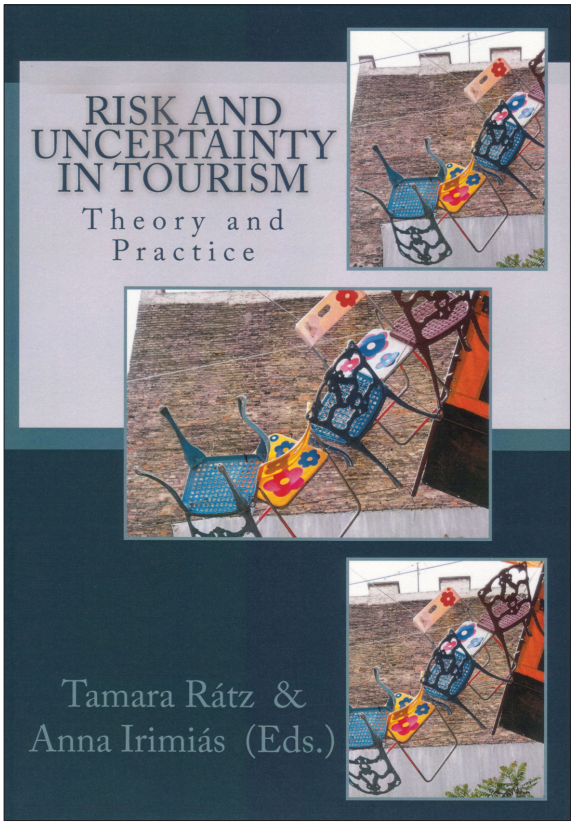

During the summer of 2012 a new volume of studies was published as a result of a cooperation between the Kodolányi János University of Applied Sciences and the Egyptian October 6. University, located at 6th of October City, a satellite city of Cairo. The chapters of this study book written in English were composed by international and Hungarian authors and they discuss several different aspects of the uncertainty and risk within field of tourism.

Hearing the words uncertainty, risk and risk management in connection with tourism, we tend to associate them with some sort of outer negative effect or threat such as terrorism or attacks on tourists whilst they are abroad. This book wants to avoid that negative tendency. Furthermore, with its 11 chapters, it explains a wide range of potential risks and uncertainty factors via a number of interesting cases.

policies alone. Environmental challenges should be assessed in the context of other global challenges such as food and energy security and poverty reduction. As many of the environmental problems are global in nature (e.g. biodiversity loss, climate change) or linked to the trans-boundary effects of globalisation, international co-operation is indispensable to ensure an equitable sharing of the cost of necessary measures.

The *OECD Environmental Outlook to 2050* with its very rich analytical background provides policy-makers, researchers and interested readers with guidance how to address more complex and long-term global environmental challenges and to enhance preventive, effective and efficient environmental policies for better and cleaner future of our children and grandchildren.

István Pomázi

Rátz, T. and Irimiás, A. eds.: Risk and Uncertainty in Tourism: Theory and Practice. Kodolányi János University of Applied Sciences, Székesfehérvár, 2012. 146 p.

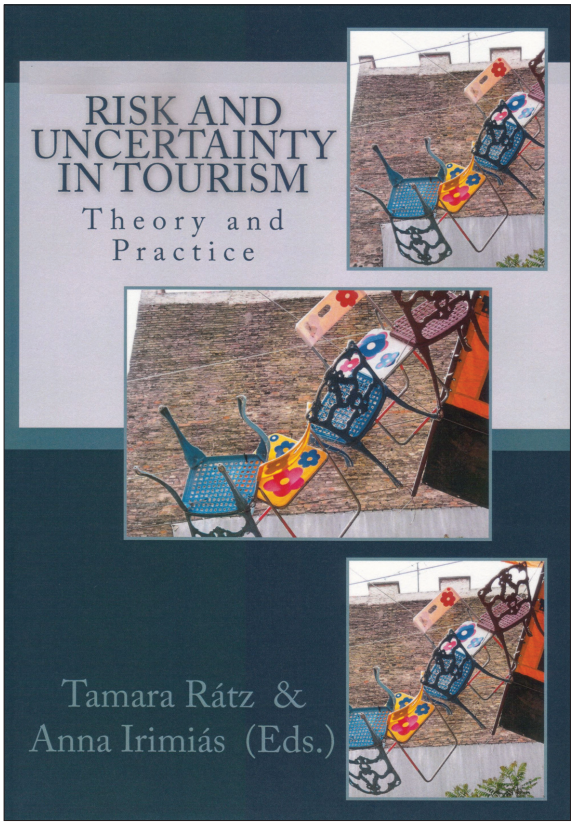

During the summer of 2012 a new volume of studies was published as a result of a cooperation between the Kodolányi János University of Applied Sciences and the Egyptian October 6. University, located at 6th of October City, a satellite city of Cairo. The chapters of this study book written in English were composed by international and Hungarian authors and they discuss several different aspects of the uncertainty and risk within field of tourism.

Hearing the words uncertainty, risk and risk management in connection with tourism, we tend to associate them with some sort of outer negative effect or threat such as terrorism or attacks on tourists whilst they are abroad. This book wants to avoid that negative tendency. Furthermore, with its 11 chapters, it explains a wide range of potential risks and uncertainty factors via a number of interesting cases.

The book consists of two parts. The first one discusses the matter of risk management in tourism as a whole process, including crisis prevention, the effects of the already developed hazard situations and the solutions of them. The longer second part uncovers the uncertainty factors of tourism, the understanding of these are crucial for the effective tourism management via six practical examples.

The studies within the book are even more emphasized by the fact that the authors honestly discuss questions in which they were personally involved (for example, the Egyptian authors write about the attacks against the Egyptian tourists). Understandably, those actions must have had a great emotional impact on them, nevertheless, they wished to share their experiences, thoughts and the methods of their problem resolution with the readers.

The following six cases presented in the book are all exciting, readable and they are especially good examples on the subject of risk management:

Proactive Crisis Management in the Hotel Industry – Practical Tips for Hotel Managers. The conclusion of the study comes from a series of interviews with Chinese, English and Finnish hotel managers and it explains five important practical steps with the help of which crisis situations could be handled in a more effective way.

Tourism and Security in the Shadow of Terrorism. The study gives a complex picture of the effect of terrorism on tourism. Additionally, it describes those effects in each main sector of tourism (transportation, hotel industry, travel agencies, insurance companies, security policies and media). Moreover, it presumes the possibility of terror attacks in different regions.

Tourism as Solution – Perceived Risks Influencing Participation in Health-related Tourism. In this study the Reader meets another kind, individual, inner assumption type of risk. This chapter follows the consumer society´s growing need for health awareness (prevention) and the reduction of health risks factors, the effect of those on health tourism and the reasons causing those tendencies to develop.

Trust. The key factors of successful tourism management and competitiveness. The success of a destination, a tourism product can be explained by the effectiveness of the cooperation between the suppliers, which is based on mutual trust between the partners. The study describes the elements of trust through a multidisciplinary analysis on the example of urban tourism.

Businesswomen on the Move – An Expanding Segment's Lodging Expectations. The present study draws attention to an interesting segment and the associated risk: it is essential for the hotels to meet the expectations of businesswomen. Since most of the decisions regarding travel are made by women, a positive/negative experience gained during a business trip can significantly influence, for instance, a businesswoman's choices on hotels and programmes, even when she is travelling with her family as a leisure tourist. The value of the study lies in presenting the characteristic travel habits and expectations of this tourism segment, and thereby it is pointed out what the individual accommodations have to prepare for.

Risk and Uncertainty Associated with Pet Ownership and Travelling. This interesting study considered to be a niche study both in the Hungarian and in the international literature reveals the uncertainty and risk factors of travelling with pets and the influential role of pets in travel decisions and the choices of destinations. In addition, the study also contains quantitative analysis about the demographic characteristics of that segment, the choice of means of transport and the characteristics of pet friendly hotels, as well.

Altogether, the study is a valuable, well-structured niche work considering the theme. It shows a wide spectrum of risk and uncertainty factors by processing exciting Hungarian and international case studies providing sufficient quantity and quality of

knowledge for the Reader. Although some of the empirical studies were made several years ago, those former statistics do not interfere with the processability of the topics and the making of conclusions.

The knowledge collected by the book is useful both in practice and in the academic area and it could be a great starting point for tourism managers, tourism educators, college and university students interested in the field of tourism.

Noémi Kulcsár

Salamin, G., Kohán, Z., Dobozi, E. and Péti, M. eds.: Climate-Friendly Cities. A Handbook on the Tasks and Possibilities of European Cities in Relation to Climate Change. VÁTI, Budapest, 2011, 268 p.

This handbook was published within the framework of the Hungarian Presidency of the Council of the European Union and geographers working both in human and physical geography can use it as a major source of knowledge in the field. Cities are not only the major challenge, but also the possible solution to climate change. According to estimations, cities use about two-thirds of the final energy demand and generate up to 70 percent of all CO_2 emissions. To reduce these shares and combat the negative effects of climate change is a great challenge.

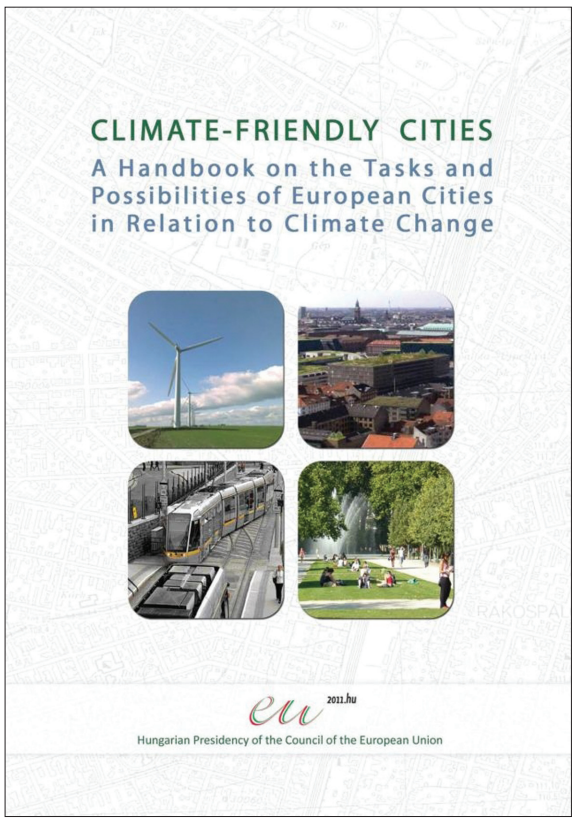

The handbook is more than timely. With the Europe 2020 strategy, the European Union has set itself the ambitious goal of recovering European economy and tackling challenges like climate change and growing energy consumption at the same time. There is a solid link between cities and Europe 2020, because cities are the driving forces of economic growth, and it is also in urban areas where a great potential for energy saving lies. Green businesses and eco-innovation can create new jobs and reduce CO_2-emissions at the same time. Investment in eco-efficient urban infrastructures ena-

knowledge for the Reader. Although some of the empirical studies were made several years ago, those former statistics do not interfere with the processability of the topics and the making of conclusions.

The knowledge collected by the book is useful both in practice and in the academic area and it could be a great starting point for tourism managers, tourism educators, college and university students interested in the field of tourism.

Noémi Kulcsár

Salamin, G., Kohán, Z., Dobozi, E. and Péti, M. eds.: Climate-Friendly Cities. A Handbook on the Tasks and Possibilities of European Cities in Relation to Climate Change. VÁTI, Budapest, 2011, 268 p.

This handbook was published within the framework of the Hungarian Presidency of the Council of the European Union and geographers working both in human and physical geography can use it as a major source of knowledge in the field. Cities are not only the major challenge, but also the possible solution to climate change. According to estimations, cities use about two-thirds of the final energy demand and generate up to 70 percent of all CO_2 emissions. To reduce these shares and combat the negative effects of climate change is a great challenge.

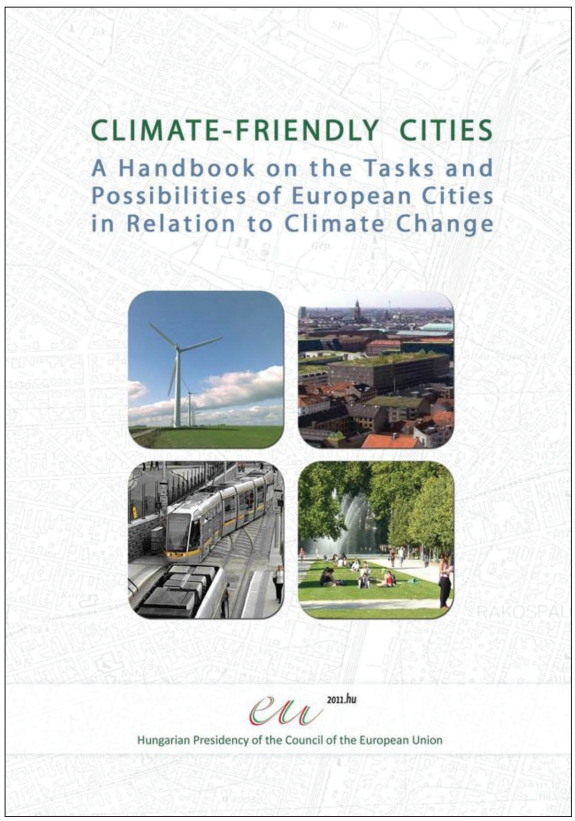

The handbook is more than timely. With the Europe 2020 strategy, the European Union has set itself the ambitious goal of recovering European economy and tackling challenges like climate change and growing energy consumption at the same time. There is a solid link between cities and Europe 2020, because cities are the driving forces of economic growth, and it is also in urban areas where a great potential for energy saving lies. Green businesses and eco-innovation can create new jobs and reduce CO_2-emissions at the same time. Investment in eco-efficient urban infrastructures ena-

bles these businesses to grow and proved jobs for more and more people. Climate change and related urban responses have become part of the European policy making by now. This is reflected by a range of policy-relevant documents like the Leipzig Charter on Sustainable European Cities, adopted in 2007, or the Toledo Declaration, adopted in 2010. These documents draw the attention to the possible role of cities in climate change adaptation, to the need for increasing energy efficiency of our cities, and to the improvement of urban infrastructure enhancing climate-friendly urban development.

This book was prepared first of all for decision makers, public officials working in city administrations, but it can also be used by researchers and students who are interested in urban geography and more specifically in the topic of climate-friendly cities. The main objective of editors was to take account of the possible means that can be used in the mitigation of and adaptation to the consequences of climate change in urban areas. This target was achieved with the collection of best practices elaborated and implemented by various European cities, providing a toolkit for city management. This approach allowed only a limited amount of in-depth knowledge or theoretical analysis; nevertheless, the case-studies included in this volume provide a useful set of possible practical actions when one think of his or her city. With the aid of the virtual library of the European Urban Knowledge Network (EUKN, www.eukn.org) the editors were able to base the handbook on a large number of technical documents and best practices implemented by various European cities.

The handbook starts with the identification of the phenomena of urban climate, its peculiarities, and the possible impacts of global change on it. The subsequent chapter focuses on possible forms of climate-friendly urban governance. The authors believe that successful governance for climate-friendly cities should be multilevel and it should encompass integrated planning as well as partnership among actors of climate protection. Chapter 3 offers an *innovative methodology* to support the *elaboration of integrated strategies*. Step by step guidance is provided city managers how to integrate climate aspects in strategic planning. The remaining ten chapters focus on different impacts of climate change and their possible mitigations in cities: such as the *urban structure* and *land use* (Ch. 4), *transportation* (Ch. 5), *low carbon energy management* (Ch. 6), *climate related architecture* (Ch. 7), *water management* and *communal infrastructure development* (Ch. 8), *disaster management* and *health care* (Ch. 9), *climate conscious behaviour* and *lifestyle of local inhabitants* (Ch. 10), *assistance of deprived social groups in adapting to climate change* (Ch. 11), *impacts of climate change on urban economy* (Ch. 12) and *urban society* (Ch. 13). Among the different sectors of urban management dealt with in the chapters, however, there are three key pillars, which have more horizontal and outstanding importance: *appropriate urban governance, climate conscious urban planning and climate-friendly urban development*. These pillars have outmost importance on the road towards climate-friendly cities.

Though this is not an academic book in its purest sense, nevertheless, we recommend it also specialists working in the academia because of its integrated approach and practical focus, which is often lacking in current academic discourses.

Zoltán Kovács

Hungarian Geographical Bulletin 61 (4) (2012) pp. 349–353.

International Conference on Water resources and wetlands

Tulcea, 14–16 September 2012

The organizers of the conference were the Romanian Limnogeographical Association (ARLG), the Danube Delta Biosphere Reserve Authority, the Danube Delta National Institute for Research and Development, supported by a series of universities (Salford, Bucharest, Iaşi, Cluj-Napoca, Târgovişte, Suceava) and academic institutions (e.g. National Institute of Hydrology and Water Management). The goal of the meeting was to present the findings of recent geographical investigations of lakes and wetlands. Participants arrived from more than 30 countries (including France, Austria, Brazil, Russia, Turkey, Japan, Iran, the United Arab Emirates and many others). (The organizers had reckoned with even more international participations, but unfortunately many foreign visitors cancelled their trip.) Hungary was also well represented by researchers of the Limnological Institute in Tihany, Hungarian Academy of Sciences, and from the Institute of Environmental Sciences, University of Pécs. The venue was the elegant Hotel Delta on the Danubean promenade of Tulcea, which has been recently supplemented with a four-star wing.

The conference venue: the Hotel Delta

Professor Petre GÂŞTESCU is greeting conference participants at the opening ceremony

Riparian willow groves along a distributary channel of the Sulina Branch

Several surprises could be recorded during the conference. For Hungarians, the first of them was the observation that in Romania – as opposed to Hungary – limnology is not only a biological or ecological discipline but an organic part of physical geographical research too. Under the guidance of Petre Gâştescu, member of the Romanian Academy of Sciences, a populous group of geographers are engaged in limnogeographical investigations and remarkable achievements could be presented. Dozens of papers of this kind are printed as extended abstracts in the voluminous conference proceedings of 662 pages.

The plenary papers of diverse topics were followed by lectures arranged in five sections: the ecology of river and lake ecosystems, climate change and water resources, coastal environments, deltas and wetlands and water policy – all highly actual fields of study with wide-scale practical applications.

Another pleasant surprise was the cultural programme associated with the festive dinner. The folk dance traditions of Romania and particularly of the multi-ethnic Dobrogea region were presented to us by a folk group.

The last day also brought an experience that will be long remembered by all participants. A whole-day boat trip to the Danube Delta in hot summer weather with temperatures above 30°C allowed us an insight into the life of this huge wetland. Our boat followed the Sulina branch navigation route half way to the Black Sea, to the centre of the cut-through meanders popularly called the Big M. From there we followed some distributary channels back to Tulcea. The boat moved with reduced speed so that we could enjoy the environment and birdlife (counting 17 species – including the overflight of several swarms of magnificent pelicans, a major attraction of the Delta).

For the successful organization gratitude is due to Academician Gâştescu, Gheorghe Romanescu, professor of the University Alexandru Ioan Cuza in Iaşi and the coordinator of all tasks, secretary of the Organizing Committee, Petre Breţcan.

Dénes Lóczy

Bernard J. Smith
(1951–2012)

In the 1980s Hungarian physical geography much profited from the assistance of the British Geomorphological Research Group, its members visited us on several occasions. The British–Hungarian Geographical Seminars also provided an excellent framework for getting new information on international research trends, consultations on various topics and also field trips to interesting sites. To the trip to the Giant's Causeway (Northern Ireland) in 1982 our Bernie Smith from the Queen's University of Belfast accompanied us. He proved to be a knowledgeable guide with humour and kindness. He remained to be associated with Hungary and included Budapest among the study sites of his urban stone weathering experiments (along with Rio de Janeiro, Venice, Prague, Dublin). With his students he also did field work in the loess and granite regions of Hungary.

The first disturbing news of his serious illness reached me when he did not respond to my Christmas card last year. And now a sad message came that he passed away on 31 October 2012 – exactly on my birthday. He was only 61 years old.

Bernie was a geographer, enthusiastic about geography both as a scientific discipline and a school subject. This means that he could not separate the researcher in himself from the teacher. As a geographer always hungry for new experience, he travelled widely in the world to gather first-hand information and impression on as many spectacular landscapes of the globe as he could.

On completing his university education at Reading in 1975, he chose to start his career in northern Nigeria, at the Ahmadou Bello University of Zaria and spent four years there. Grasping an opportunity to work in the United Kingdom, he joined the staff of Queen's and settled in Belfast. When I asked him in the late eighties whether living in this city of constant turmoil or even street fighting involved some danger for him, his reply was that he had never ever seen any religious clashes during his stay there. Working with Professor Brian Whalley, he became head of the Department of Tropical Geomorphology and held this position from 1979 to 2011, when he had to retire early because of his illness.

Within geomorphology Bernie's interests ranged on a wide scale: he fell in love with the arid environments at an early age, and to this were added his curiosity in desert processes (granite weathering, dust and loess formation) but also deep weathering in the humid tropics and similar processes under Mediterranean climate. Within the School of Geography, Archaeology and Palaeoecology in the early 1990s he established a specialized research unit, the Weathering Research Group. This allowed him to start international investigations embracing many countries and numerous links to human geography, since the study of building stones decay involves aspects of architecture, urban planning, cultural heritage, archaeology, history and many others. The interdisciplinary contacts brought him

many friends in all parts of Europe and – through his participation at conferences – also in other continents. He also became associated with the UNESCO's Natural World Heritage programme and worked as an evaluator. Among his achievements is the inscription of the Giant's Causeway on the list of the heritage sites.

Along with the members of his family, his wife, Dorothy, and children, Daniel and Catherine, Bernie must be best remembered by his students, who follow in his steps and teach with great enthusiasm not only at Queen's but also at the various universities of the United Kingdom and the world. The older generation of Hungarian geomorphologists will also keep him in good memory and feel gratitude for the conversations with him on both academic and every-day topics, which gave us insight into his modest but wise, somewhat secluded but kind personality. May you rest in peace, Bernie.

Dénes Lóczy